UIDE

Powered by Arizona State University

ING. MECATRÓNICA

Tesis previa a la obtención del título de Ingeniero en Mecatrónica.

Autor: Arévalo Castro, José Alfredo

Tutor: Mosquera Canchingre. Guillermo Alfredo

PROTOTIPADO BRAZO ROBÓTICO SOLDADURA

WELDING ROBOTIC ARM PROTOTYPE

Quito-2026

CERTIFICATE OF AUTHORSHIP

I, Jose Alfredo Arévalo Castro, hereby declare that this submission is my own work, it has not been previously submitted for any degree or professional qualification and that the detailed bibliography has been consulted.

I transfer my intellectual property rights to the Universidad Internacional del Ecuador, to be published and divulged on the internet, according to the provisions of the Ley de Propiedad Intelectual, its regulations and other legal dispositions.

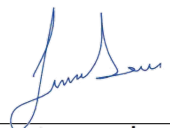

JOSE ALFREDO AREVALO CASTRO

APROBACIÓN DEL TUTOR

Yo Guillermo Mosquera Canchingre, certifico que conozco al autor del presente trabajo de titulación denominado “Prototipado Brazo Robótico Soldadura”, José Alfredo Arévalo Castro, siendo el responsable exclusivo tanto de su originalidad y autenticidad, como de su contenido.

.....

DIRECTOR DEL TRABAJO DE TITULACIÓN

ACKNOWLEDGMENTS

First and foremost, I thank God for granting me the strength, health, and wisdom necessary to complete this stage of my life and to overcome every obstacle along the way.

To my parents, María Castro and Manuel Arévalo, the true engines of my life. Thank you for your unconditional love, your tireless sacrifices, and for always believing in me. This achievement is as much yours as it is mine.

To my brother, Víctor Arévalo, for his unwavering support, and to my niece, Victoria Arévalo, for being a constant source of joy and inspiration that motivated me to keep going.

I extend special gratitude to my supervisor, Guillermo Mosquera, for his accurate guidance, patience, and for sharing his technical expertise during the development of this project.

Likewise, I express my sincere appreciation to Vladimir Félix, Samuel Peña, Sebastián Tamayo, and Marcelo Moya, who significantly enriched the development of this project with their constructive comments and key insights.

To my friends and university classmates, who were a fundamental pillar throughout my studies. Thank you for the shared study hours, your moral support, and above all, for those timely corrections and pieces of advice that helped me improve.

To the Universidad Internacional del Ecuador, my alma mater, for opening its doors to me and providing the knowledge and tools that today shape my professional profile.

CONTENTS

LIST OF FIGURES

LIST OF TABLES

Chapter 1

INTRODUCTION

Technological evolution has fundamentally transformed industrial environments, driving the transition towards Industry 4.0. This paradigm shift prioritizes not only production efficiency and cost reduction but also the maximization of product quality and safety. Within this context, robotic manipulators have emerged as indispensable tools, capable of replicating and often surpassing human dexterity in repetitive or high-precision tasks across sectors such as manufacturing, medicine, and research [1, 2].

Specifically in the field of metalworking, arc welding is a critical process that demands strict adherence to technical standards. Regulations such as the AWS D1.1 code, established by the American Welding Society [3], define precise guidelines for structural steel welding. Achieving compliance with such rigorous standards through manual operation is increasingly challenging due to human fatigue and variability. Consequently, automation through robotics becomes essential to maintain the consistent parameters—such as speed and trajectory—mandated by these regulations.

To address these challenges, Six-degree-of-freedom (6-DOF) robotic arms represent a significant technological solution. By providing a three-dimensional workspace with complex rotations and transitions, they simulate the kinematics of a human arm, making them ideal for executing intricate welding trajectories such as circular or linear paths with high repeatability [4, 5]. However, the implementation of such technology presents operational challenges for Small and Medium-sized Enterprises (SMEs), which often lack the capital to invest in physical robotic infrastructure. This financial limitation hinders their ability to perform precise trajectory analysis and production optimization.

To bridge this gap, and in collaboration with the company CNESTRONIC, this project focuses on developing a high-fidelity virtual prototype of a 6-DOF robotic arm with a workspace of approximately 1 m^3, specifically engineered for welding applications. A critical aspect of this proposal is the adherence to recognized industrial parameters. The system is designed to validate specific welding requirements, such as a continuous

welding dimension of 3.2 mm (equivalent to 1/8 inch standards) and an intermittent welding spacing of 40 mm. These values, based on technical infrastructure norms [6] and aligned with standards like AWS D1.1 [3], serve as a benchmark to guarantee the feasibility of the welding process before any physical implementation, significantly reducing development risks [7].

Therefore, the project adopts an exclusively virtual phase utilizing SolidWorks and MATLAB to model, simulate, and validate kinematic behavior. This methodology serves a dual purpose: it supports the technical validation supported by recent simulation studies [8, 9], and fulfills a vital educational role by training mechatronic engineers in complex areas such as inverse kinematics and trajectory control within a safe environment [10]. Ultimately, this establishes a robust foundation for future physical implementations, integrating improvements such as artificial intelligence algorithms for trajectory optimization.

Based on the identified needs and the proposed technological solution, the general objective of this project is to develop a robotic arm capable of performing welding tasks automatically, accurately, and safely through simulation.

To fulfill the general objective, the following specific goals have been proposed:

- Design a robotic arm capable of performing welding tasks, considering its structure, components, and control system.
- Develop forward and inverse kinematic models of the robotic arm to precisely control its movements within the simulation environment.
- Validate the operation of the simulated model through virtual testing to evaluate its accuracy and performance.

Chapter 2

METHODOLOGY AND DESING

The design of the robotic arm followed the VDI 2206 methodology. This framework organizes the development into seven sequential phases, ensuring a structured progression from requirements definition to virtual validation, as shown in Figure 1.

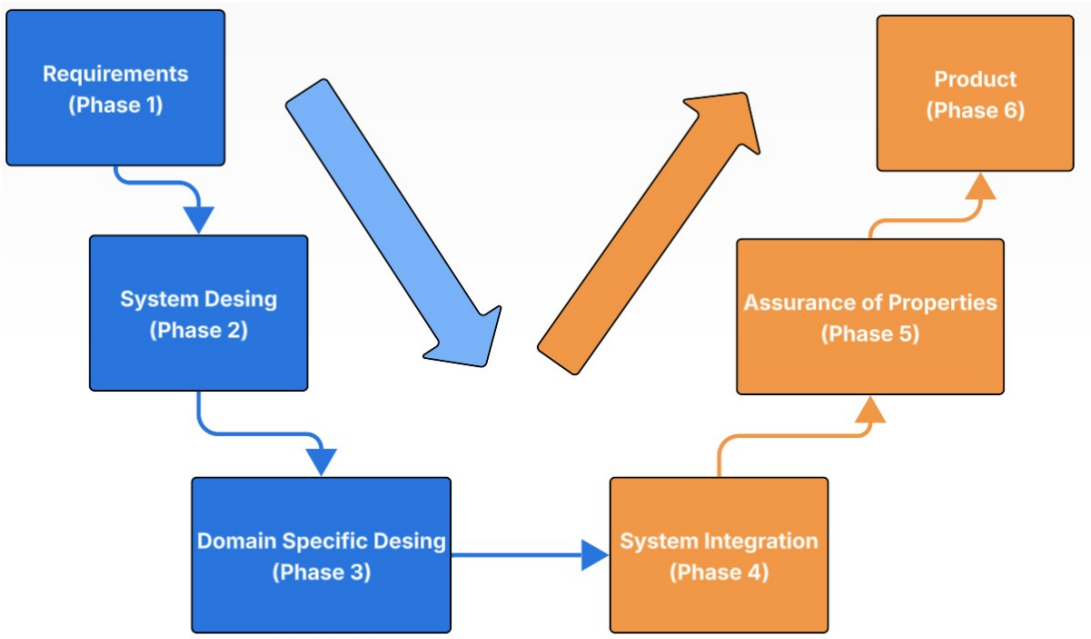

Figure 1. Project workflow based on the VDI 2206 V-Model.

As detailed in Figure 1, the workflow is organized into a continuous stream divided into three main stages. The descending branch (Phases 1–3) focuses on the definition and design of the system, translating high-level requirements such as a 1 m^3 workspace and a 5 kg payload into a specific anthropomorphic configuration and the detailed selection of mechanical and electrical components. The vertex of the ”V” represents the core implementation stage, where mathematical modeling and kinematic analysis are executed within the MATLAB environment. Finally, the ascending branch (Phases 4–6) addresses the virtual verification of the system, starting with kinematic integration and path planning, followed by rigorous property assurance to ensure torque limits remain below 450 Nm, and culminating in the delivery of a fully validated virtual prototype optimized for automated MIG welding tasks.

2.1. STAGE I: SYSTEM DEFINITION AND DESIGN

2.1.1. Application of the VDI 2206 Methodology

After defining the project, the VDI 2206 methodology was selected as the framework for designing the 6-DOF robotic arm for MIG welding. This methodology structures the development and defines the key system requirements:

1. **Functional Requirements**
    - Follow planned trajectories accurately.
    - Move smoothly during continuous operation.
    - Move from one position to another in point-to-point mode.
    - Perform automated welding tasks.
2. **Non-Functional Requirements**
    - The trajectories to be followed are a square, a circle, and a linear path along the z-axis.
    - The robotic arm must be designed to support a payload of at least 5 kg at the end effector.
    - The system must maintain a constant linear velocity at the end effector during trajectory execution.
    - The system must be modular to allow for quick changes without having to break or rebuild the entire robot.
3. **Design Constraints**
    - The manipulator must have six degrees of freedom (6-DOF) to reach the required positions and orientations within the workspace.
    - Limitations in materials for the prototype, considering the use of ABS and aluminum.
    - Maximum working reach is defined as $1\,\mathrm{m}^3$.

- Development is limited to a virtual prototype during this phase, without physical construction.
- Exclusive use of free or educational software platforms (MATLAB/Simulink, SolidWorks Student, Fusion 360).

2.1.2. System Requirements Definition

The development of this project is based on the preliminary requirements, which allow for the simulation of a 6-degree-of-freedom robotic arm. The following requirements are presented:

- The robotic arm must reach a size of 1 m^3 in accordance with CNESTRONIC's specifications.
- The robotic arm must have six degrees of freedom to perform tasks remotely, with the aim of reducing workers' exposure to hazardous environments.
- This project must be carried out in simulation.

2.1.3. Architectures according to the VDI 2206 methodology

1. **Functional Architecture:**

   This stage defined the functional architecture required for the effective operation of the robotic arm. The process begins with the input of the desired trajectory, which is processed by the control center to drive the actuators. Subsequently, through the application of forward and inverse kinematics, the physical output trajectory is executed based on the initial configuration parameters. These functions work synergistically to ensure precision, repeatability, and safety during the welding process, as illustrated in Figure 2.

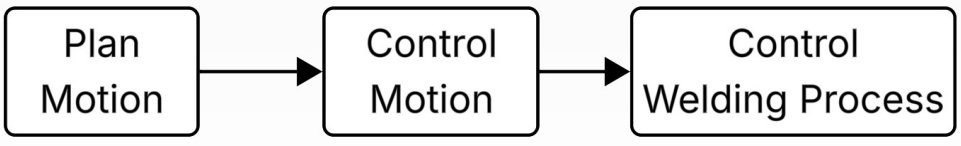

Figure 2. Functional architecture of the 6 dof.

2. **Logical Architecture:**

This stage defines the information exchange protocol between the robotic arm subsystems. The operation begins with the transmission of the desired trajectory, prompting the control system to execute the necessary kinematic calculations to drive the mechanical actuation. Simultaneously, the sensor system detects the actual motion and provides feedback to the control system, which adjusts the parameters to ensure the output aligns with the desired final trajectory. The corresponding logical architecture is shown in Figure 3.

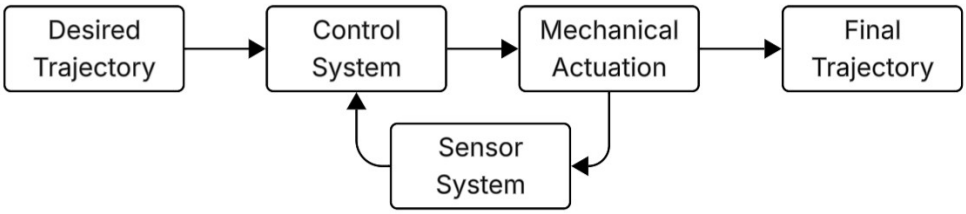

Figure 3. Logical architecture of the 6 dof.

3. **Physical Architecture:**

The robotic arm in this architecture is based on the specific organization of the elements that will be used if implemented, where the power supply provides energy to both the microcontroller and the drivers responsible for activating the motors distributed in each joint involved, which are “waist, shoulder, arm, forearm, doll, and hand.” The microcontroller receives instructions from the computer running the code, sends control signals to the drivers, and receives feedback from the sensors associated with each motor, allowing for closed-loop control of position and movement. Although the system is developed in a simulation environment, a structural representation equivalent to that of a real robotic arm is established for each link and joint. The integration of these elements within the simulation platform allows for the analysis of kinematic behavior, verification of trajectories, and validation of control strategies without requiring physical hardware, as shown in Figure 4.

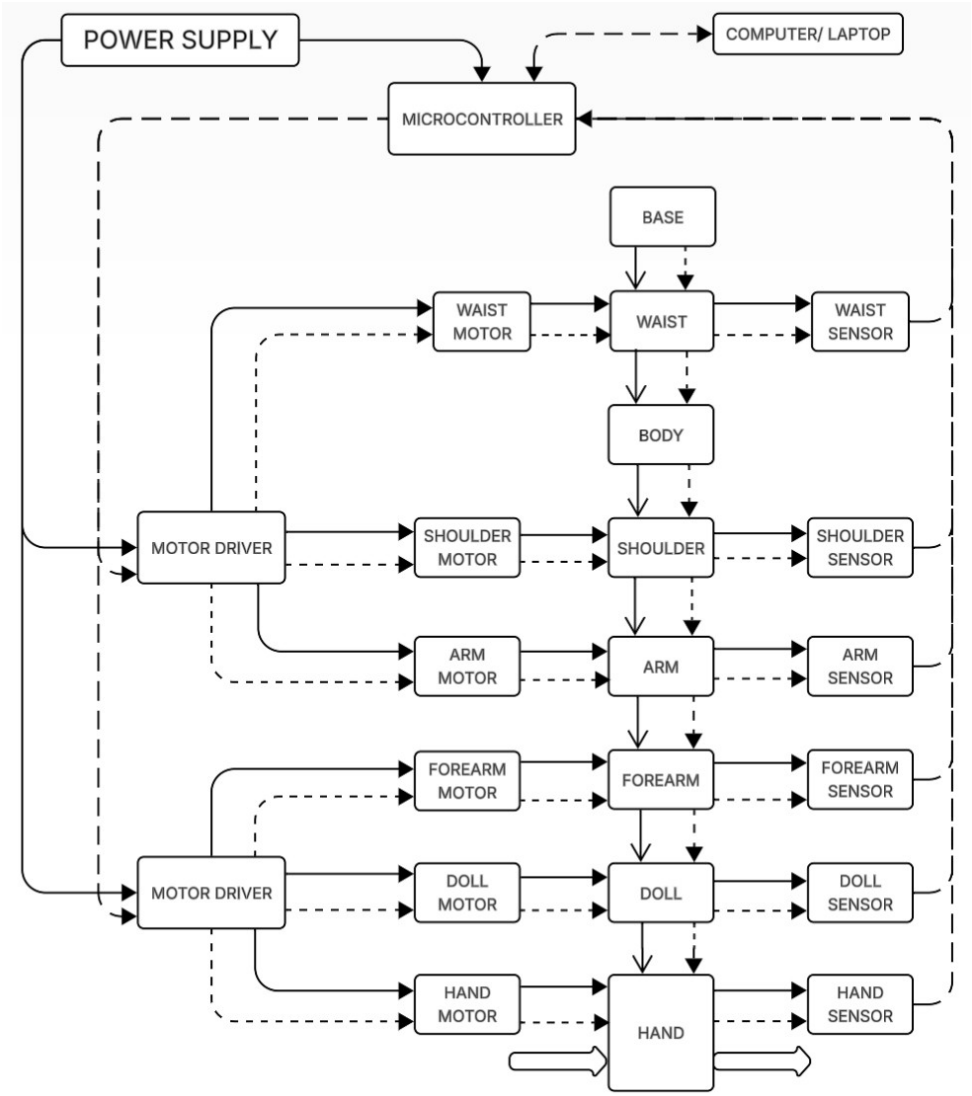

Figure 4. Physical architecture of the 6 dof.

2.1.4. Conceptual Manipulator Design

The proposed manipulator is based on a 6-degree-of-freedom (6-DOF) configuration, chosen for its versatility in welding [7] and adaptability to manageable scales [11, 12]. Given the high costs of industrial equipment, the literature supports the design of modular and accessible educational prototypes [1, 10, 13–16]. To illustrate this motion architecture, Figure 5 presents the theoretical kinematic diagram alongside its implementation in the simulation environment, visualizing the physical correspondence of each joint.

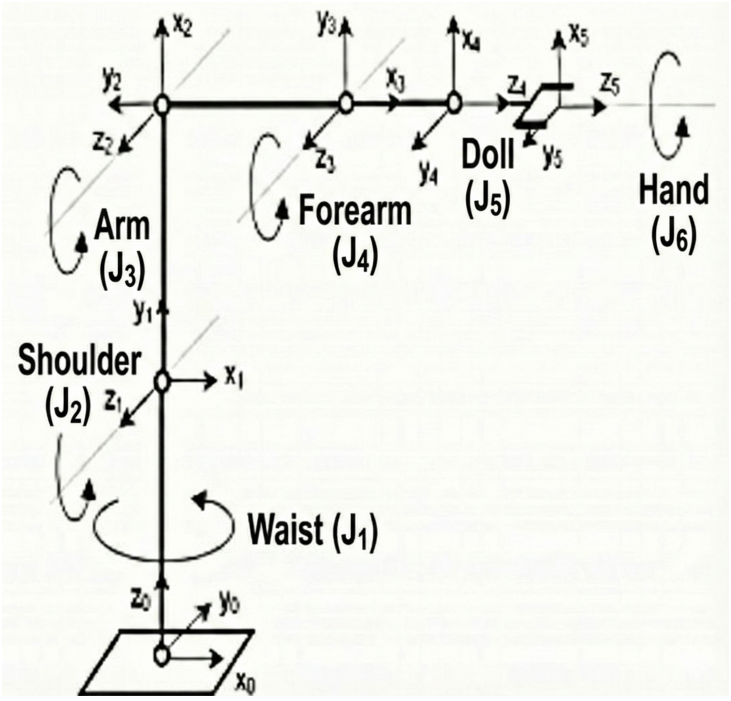

Figure 5. Kinematic diagram and simulation model of the 6-DOF arm [17].

Based on the anthropomorphic architecture detailed in Figure 5, the system consists of a serial kinematic chain composed of rotational joints and rigid links [17]. The main components are described below:

- **Joints:** The robot features 6 rotational joints (J_1 to J_6) that define its degrees of freedom:

    1. **Waist (J_1):** Allows rotation of the base around the vertical axis (z_0), defining the robot's azimuthal positioning.
    2. **Shoulder (J_2):** The joint responsible for the main lifting of the arm, acting on the horizontal axis (z_1).
    3. **Elbow (J_3):** Provides extension and flexion of the arm, complementing the vertical and radial reach.
    4. **Forearm (J_4):** Enables longitudinal rotation of the forearm, which is crucial for tool orientation.
    5. **Doll (J_5):** The joint responsible for the pitch motion of the end tool.
    6. **Hand (J_6):** Performs the final roll rotation to orient the end-effector in the welding direction.

- **Links:** Rigid elements that connect the joints and determine the robot's workspace volume. Key links include the base link, the arm link (between J_2 and J_3), and the forearm link (between J_3 and the wrist).
- **End-Effector:** Located after joint J_6, this is the mounting point for the MIG welding torch. Its position and orientation (Pose) are the result of the vector sum of all preceding movements.

2.2. STAGE II: VIRTUAL IMPLEMENTATION AND MODELING

2.2.1. Specific Design

Considering the kinematic and dynamic constraints imposed by critical welding parameters (speed, angle, and stick-out), the design was developed to maximize precision. For the development of the model in a virtual environment, the **ESTUN AUTOMATION ER20-1780-F industrial robot** is taken as a reference. This 6-DOF manipulator features a 16 kg payload capacity, a maximum reach of 1780 mm, and a repeatability of 0.1 mm, geometric characteristics detailed in Figure 6 that ensure the stability required for the process.

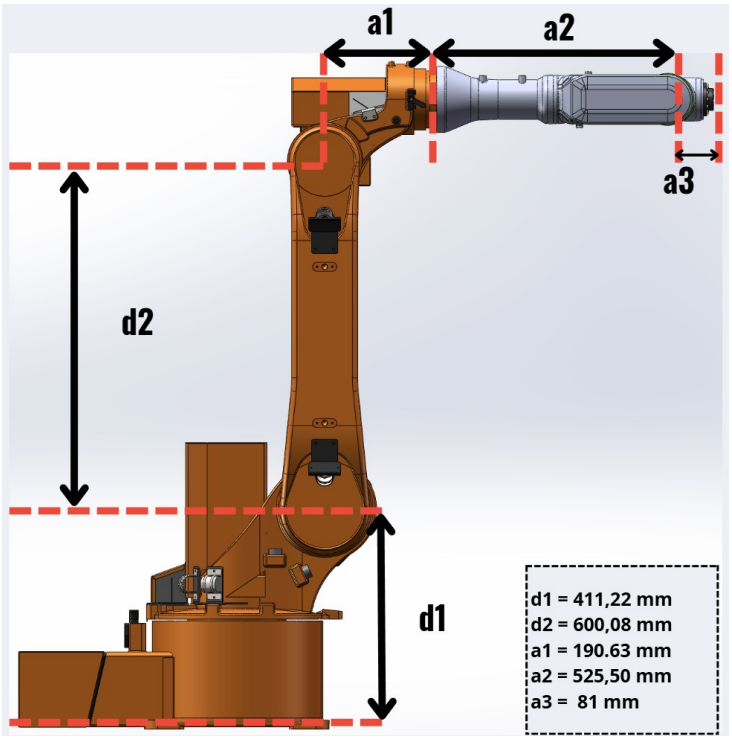

Figure 6. Dimensional Parameters of the Articulated Manipulator.

Based on this architecture, geometric modeling is performed in MATLAB using the Robotics Toolbox, a standard practice in research for manipulator simulation and validation [4, 5, 9, 18–21]. To define the system kinematics, the Denavit-Hartenberg (DH) parameters [22] are employed to establish the transformations between joints, as presented in Table 1.

Table 1. Denavit-Hartenberg Parameters of the 6-DOF Robotic Arm

Joint	$\mathbf{a_i}$ (m)	$\alpha_\mathbf{i}$ (rad)	$\mathbf{d_i}$ (m)	$\theta_\mathbf{i}$ (rad)
1	0	$-\frac{\pi}{2}$	$d1$	0
2	$d2$	0	0	0
3	$a1$	$\frac{\pi}{2}$	0	0
4	0	$-\frac{\pi}{2}$	$a2$	0
5	0	$\frac{\pi}{2}$	0	0
6	0	0	$a3$	0

Furthermore, utilizing the tools provided by the Robotics Toolbox (RTB) for MATLAB, developed by Peter Corke [23], it was possible to model and visualize the kinematic structure of the robotic arm using the defined Denavit-Hartenberg parameters. This toolbox enabled the individual manipulation of each joint, verifying that the generated movements were consistent with the established geometric configuration. The resulting visualization confirms the correct kinematic behavior of the manipulator, as shown in Figure 7. This validation allowed for the identification of the HOME point, which serves as the initial reference for executing the trajectories developed in this project.

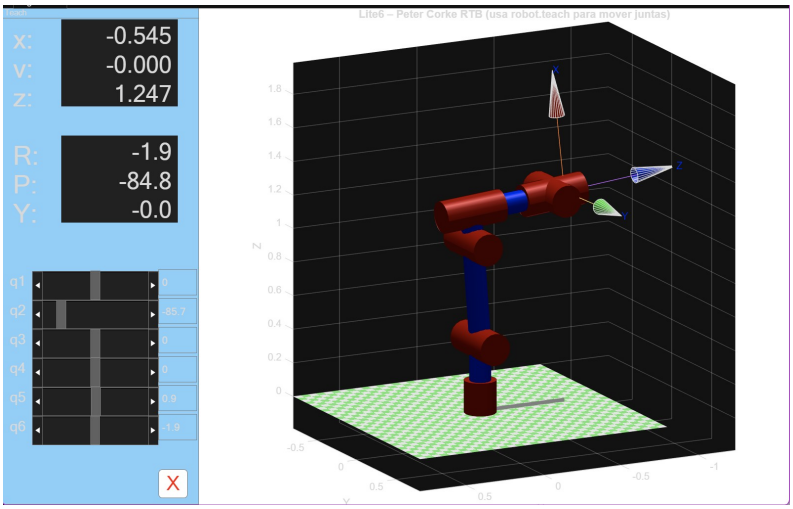

Figure 7. Control and Position View for a 6-DOF Robot using RTB.

2.2.1.1. Robotics and Welding Automation

Welding automation is crucial in industrial robotics for ensuring precision and safety. In the literature, [24] and [15] address kinematics and design for specific applications. To meet rigorous quality standards, [8] optimizes parameters through simulation, while [2] integrates machine vision for real-time trajectory control. In this context, Figure 8 illustrates the essential physical components of the MIG process required for proper execution [25].

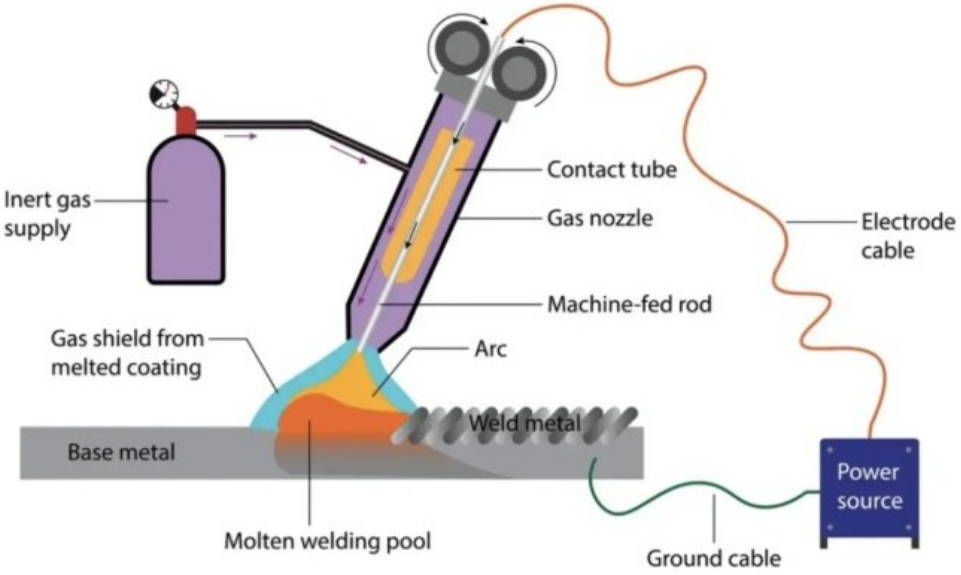

Figure 8. Structure and main components of the MIG welding process [25].

It also highlights the elements directly involved in the formation of the arc and in the protection of the molten pool, emphasizing the latter as the region of metal that remains in a liquid state under the action of the electric arc and which, with adequate gas protection, subsequently solidifies to form a stable, contamination-free bead.

2.2.1.2. Focus on Gas Metal Arc Welding (GMAW - MIG)

Among automation techniques, Gas Metal Arc Welding (GMAW), commercially known as MIG, holds a prominent position. This method utilizes a continuously fed wire electrode through a torch, alongside an inert or active shielding gas flow (argon, CO_2, or mixtures) to protect the weld pool from atmospheric contamination. Due to the nature of the process, its robotic implementation demands millimeter precision. As indicated by [1] and [8], geometric validation is a determinant of final quality; consequently, en-

suring operational stability and achieving defect-free beads necessitates the rigorous management of the following critical parameters:

- **TRAVEL SPEED:** This is the rate at which the robot moves the torch, and it is the most critical factor as it directly dictates the heat input to the metal [4]. In industrial MIG processes, this speed typically ranges between 6 and 12 mm/s (350 to 750 mm/min). Incorrect control of this parameter leads to the defects illustrated in the Figure 9.

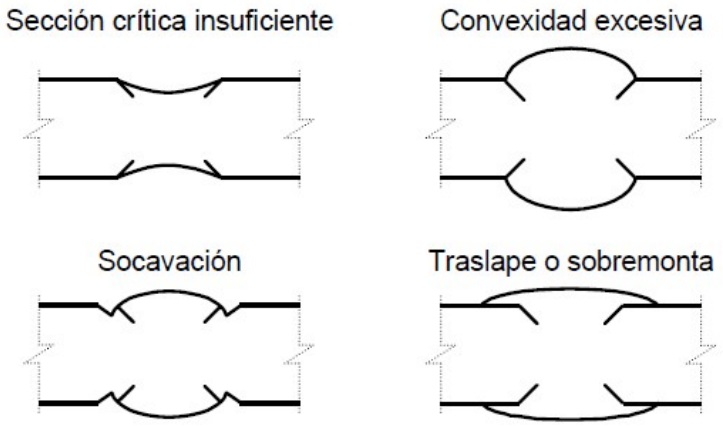

Figure 9. Defective profiles in groove welding on butt joints [6].

As shown in the figure, travel speed deviations cause structural failures: excessive speed results in incomplete fusion due to low heat input, while slow speed causes excessive convexity and undercutting. Since these defects contravene the technical fundamentals described in [6] and are direct grounds for rejection under the AWS D1.1 standard [3], operating within the established range is mandatory. To ensure this compliance, thermal simulation [8] and real-time correction algorithms [2] are essential for maintaining constant speed.

- **TORCH ANGLE:** This is a critical parameter that directly controls heat distribution, penetration, and bead morphology [1]. In robotic MIG welding, it is essential that the torch maintain a precise angle, typically between 0° and 15° relative to the perpendicular of the bead. Deviation from this range negatively impacts the uniformity of the molten pool and can cause spatter. The different types of spatter can be seen in the Figure 10.

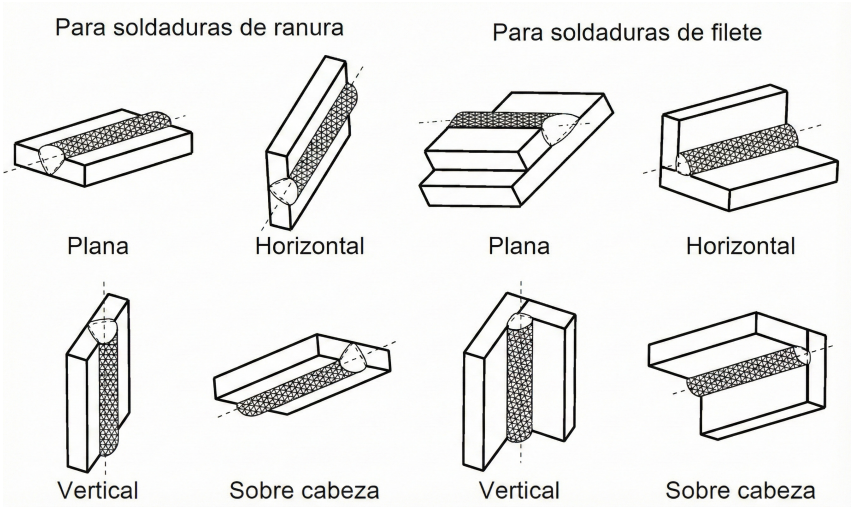

Figure 10. Positions for performing welding [6].

Given that this study will focus primarily on the Flat and Vertical welding positions, the robot's ability to maintain this precise angle will be tested under different gravitational forces. This capability represents a fundamental challenge in kinematic design, as it demands rigorous validation of its Inverse Kinematics to ensure accessibility to all welding points, even in complex geometries, as emphasized by studies such as [3, 6, 24].

- **STICK-OUT:** Defined as the wire extension beyond the contact tip, this parameter governs electrical resistance and welding current. According to [15], excessive length reduces penetration, while a short length risks overheating. Maintaining this distance requires high structural rigidity and precision, alongside dynamic control algorithms capable of compensating for geometric irregularities [4, 26].

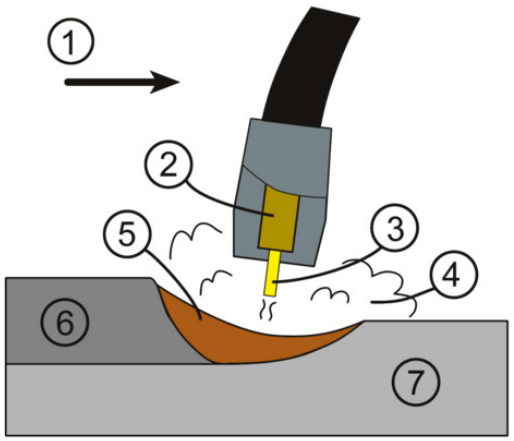

Figure 11. Positions for performing welding [26].

As illustrated in Figure 11, the welding operation proceeds along the **Direction of travel (1)**, where the stick-out is defined by the extension of the **Electrode (3)** exiting the **Contact tube (2)** towards the **Workpiece (7)**. While the **Shielding gas (4)** protects the arc environment, maintaining the correct stick-out distance is critical for thermal stability. A deviation causing an excessively long stick-out reduces the welding current, preventing the **Molten weld metal (5)** from reaching the necessary temperature to properly fuse with the base material [26]. This results in defects within the final **Solidified weld metal (6)**, specifically Incomplete Fusion. According to the standard [6], "there shall be complete fusion between the filler metal and the base metal". Any joint failing to meet this requirement due to inconsistent electrode extension must be rejected. Therefore, achieving fusion completeness is mandatory, making trajectory validation indispensable.

2.2.2. Mathematical and Kinematic Modeling

This section presents the complete mathematical framework used in the project, including the forward kinematics for obtaining the end–effector pose and the inverse kinematics for computing the joint angles required to achieve a desired pose. The model is based on the Denavit–Hartenberg parameters listed in Table 1.

2.2.2.1. Forward Kinematics

The homogeneous transformation between frames $i-1$ and i using the standard DH convention is:

$$A_i \equiv {}^{i-1}T_i = \begin{pmatrix} \cos\theta_i & -\sin\theta_i\cos\alpha_i & \sin\theta_i\sin\alpha_i & a_i\cos\theta_i \\ \sin\theta_i & \cos\theta_i\cos\alpha_i & -\cos\theta_i\sin\alpha_i & a_i\sin\theta_i \\ 0 & \sin\alpha_i & \cos\alpha_i & d_i \\ 0 & 0 & 0 & 1 \end{pmatrix}.$$

For a 6-DOF manipulator, the matrices $A_1, \ldots, A_6$ are multiplied sequentially to obtain

the full transformation from the base to the end-effector:

$$T \equiv {}^0T_6 = A_1A_2A_3A_4A_5A_6 = \begin{pmatrix} R & p \\ \mathbf{0}_{1\times 3} & 1 \end{pmatrix},$$

where $R \in R^{3\times 3}$ is the rotation matrix and $p \in R^3$ is the end-effector position. Using the joint vector $\boldsymbol{\theta} = [\theta_1, \ldots, \theta_6]$, the forward kinematics function is:

$$T(\boldsymbol{\theta}) = A_1(\theta_1)A_2(\theta_2)\cdots A_6(\theta_6).$$

2.2.2.2. Geometric Parameters and Home Position

The geometric parameters used in the model are:

$$d_1 = 0.41122 \text{ m}, \quad d_2 = 0.60008 \text{ m}, \quad a_1 = 0.19063 \text{ m},$$
$$a_2 = 0.52550 \text{ m}, \quad a_3 = 0.08100 \text{ m},$$

with twist angles:

$$\alpha_1 = -\tfrac{\pi}{2},\ \alpha_2 = 0,\ \alpha_3 = \tfrac{\pi}{2},\ \alpha_4 = -\tfrac{\pi}{2},\ \alpha_5 = \tfrac{\pi}{2},\ \alpha_6 = 0.$$

In the *Home* configuration ($\theta_i = 0$), the end–effector position is:

$$\mathbf{P}_{\text{Home}} = \begin{pmatrix} 0 \\ -(L_2 + L_3 + L_5) \\ L_1 + L_4 \end{pmatrix},$$

With numeric values:

$$L_1 = 0.41122 \text{ m}, \quad L_2 = 0.60008 \text{ m}, \quad L_3 = 0.19063 \text{ m},$$
$$L_4 = 0.52550 \text{ m}, \quad L_5 = 0.08100 \text{ m}.$$

Thus,

$$\mathbf{P}_{\text{Home}} = \begin{pmatrix} 0 \\ -0.87171 \\ 0.93672 \end{pmatrix} \text{ m.}$$

This matrix represents the initial rest position, which serves as the starting point for all control trajectories, as can be clearly seen in Figure 6.

2.2.2.3. Jacobian and Singularities

The geometric Jacobian is:

$$J(\mathbf{q}) = \begin{pmatrix} J_v(\mathbf{q}) \\ \\ J_\omega(\mathbf{q}) \end{pmatrix},$$

with

$$J_v^{(i)} = z_{i-1} \times (p_6 - p_{i-1}), \qquad J_\omega^{(i)} = z_{i-1}.$$

Singular configurations occur when the Jacobian loses rank, typically when its determinant or singular values approach zero. These configurations reduce manipulability and must be avoided during trajectory planning.

2.2.3. Programming and Control Implementation

To develop the code base used to generate and simulate the movements of the robotic arm, a structured approach was implemented, divided into two main stages: trajectory generation in MATLAB and dynamic control validation in Simulink.

2.2.3.1. Trajectory Generation and Kinematic Algorithms

The computational routine developed for this project generates precise movement commands based on the robot's kinematic model. The complete logic is structured into a unified flowchart, divided for clarity into two main stages: System Configuration and Motion Execution.

The initialization phase, illustrated in Figure 12, begins by defining the geometric constants and Denavit–Hartenberg (DH) parameters required to construct the robot's morphology and compute the **Direct Kinematics**. Subsequently, the system establishes

the operational parameters, specifically the **Speed** and the **Operating Mode** (Continuous or Intermittent). Based on the selected **Type of Career Path**, the algorithm branches into three specific motion profiles, each governed by a distinct mathematical formulation:

- **Linear Trajectory (Z-Axis):** Generated using **Linear Interpolation** equations to produce vertical displacement.
- **Circular Trajectory:** Calculated using **Trigonometric** parametric equations ($R\cos\theta, R\sin\theta$) to maintain a constant radius.
- **Square Trajectory:** Constructed using a hybrid approach where straight segments utilize **Linear Interpolation**, while corners employ **Parametric Circle Equations** for smooth blending.

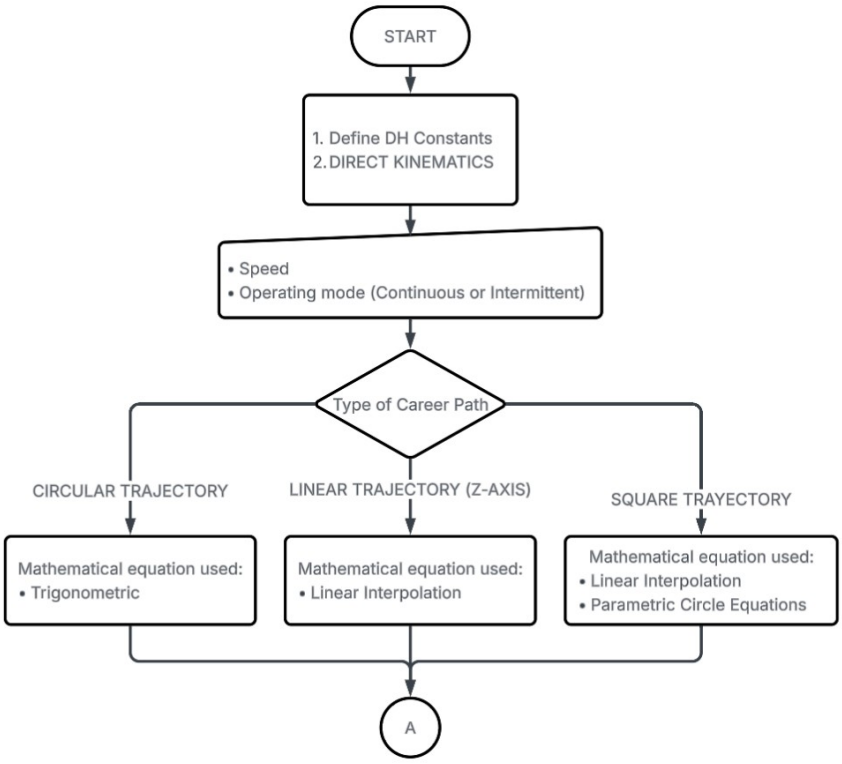

Figure 12. Flowchart Part 1: System Initialization and Geometric Trajectory Selection.

Once the geometric path is defined, the algorithm proceeds to the motion execution phase via connector ”A”, as detailed in Figure 13. To ensure mechanical safety and prevent abrupt accelerations, the initial transition from the relationship’s home position

to the starting point (**Phase 1: Approach**) is governed by a **5th Order Polynomial** equation of motion.

The core of the process is the iterative loop controlled by the decision block $k \leq N$. Here, k represents the current step index and N is the total number of points in the discretized trajectory. As long as $k \leq N$, the loop executes the following steps for the welding path:

1. **Desired Position (P_k):** The target coordinates are extracted.
2. **Constant Velocity Profile:** Time segments are calculated to maintain the user-defined speed.
3. **Inverse Kinematics:** The numerical solver (*fsolve*) computes the required joint angles (q_{sol}).

When the condition $k <= N$ is met (indicating the path is complete), the system initiates **Phase 3 (Return)**, which moves the robot back to the home relationship position using a smooth 5th-order polynomial profile. Finally, the computed joint data is consolidated and exported to the MATLAB Workspace as `theta_simulink` for simulation.

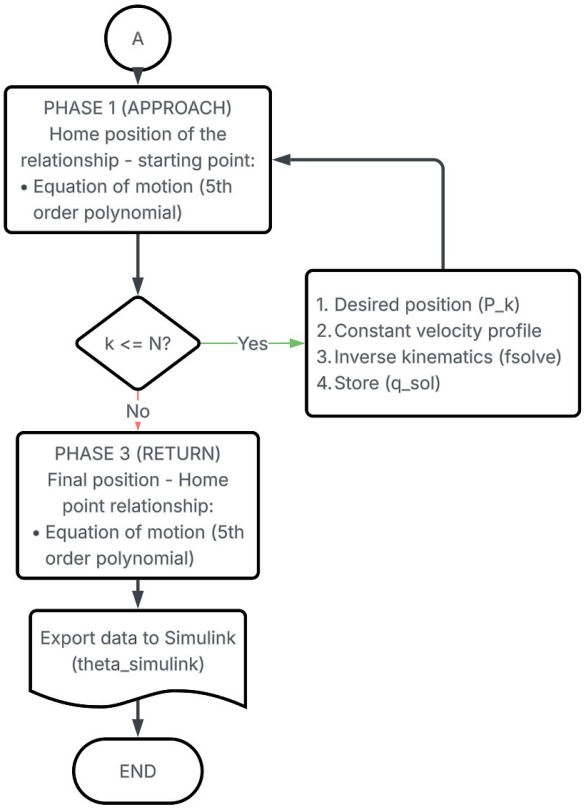

Figure 13. Flowchart Part 2: Execution Loop, Quintic Transitions, and Data Export.

2.2.3.2. Control Architecture and Simulation

Once the joint-angle signals are generated (exported as *theta_simulink*), the validation phase is conducted in Simulink/Simscape. Maintaining adequate control of end-effector speed and acceleration is fundamental for weld quality, as discussed in real-time monitoring studies [2, 27, 28]. To assess this, a comparative architecture was designed (Figure 14), where the reference signals are sent simultaneously to an “Ideal” kinematic model and a “Real” physical model that accounts for mass and inertia.

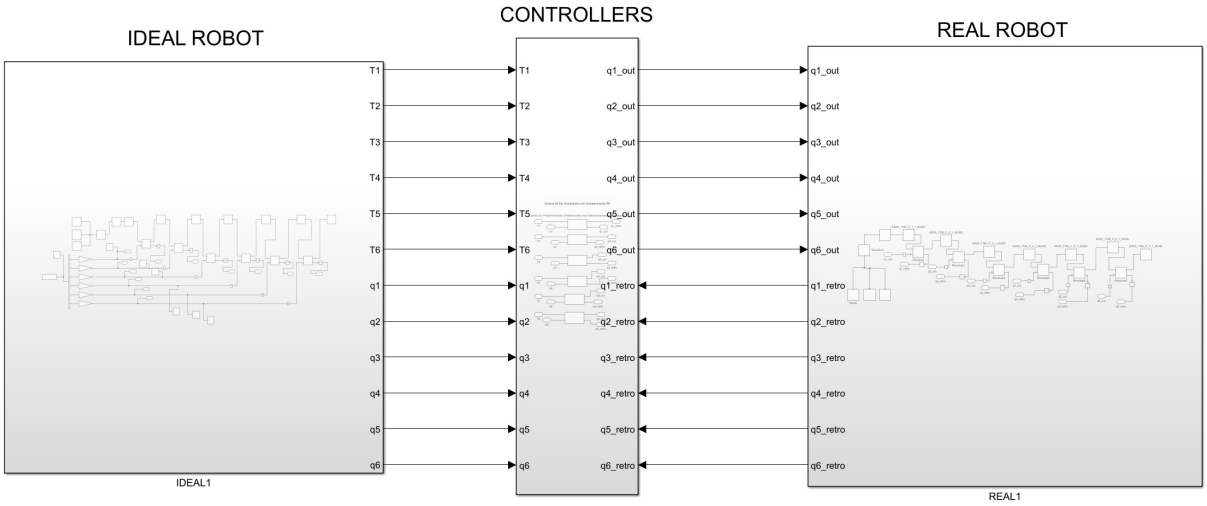

Figure 14. Simulation Architecture: Ideal vs. Real

The internal structure of the Simulink model connects the kinematic transforms with the rigid body blocks, creating a chain of coordinate systems that represents the serial arm, as detailed in Figure 15.

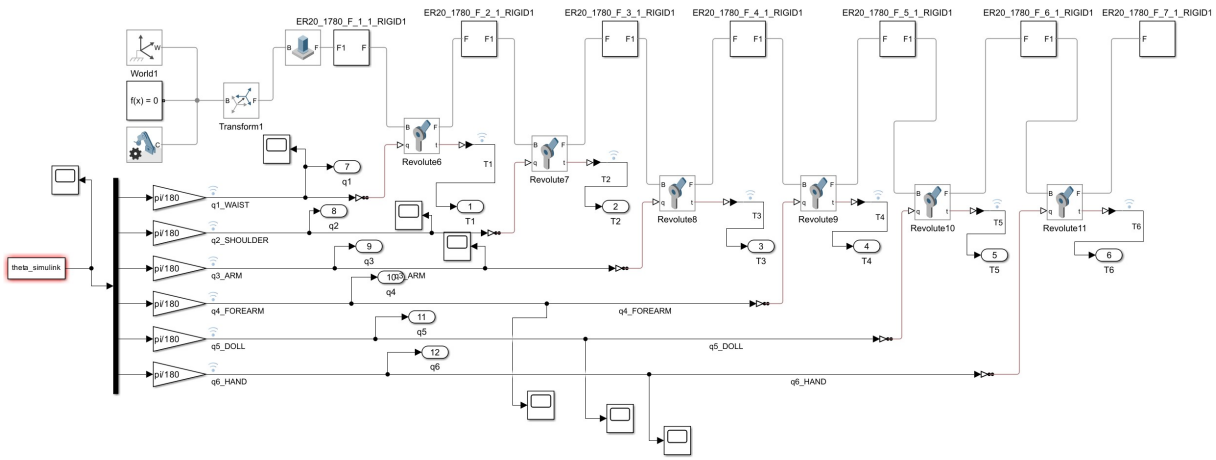

Figure 15. Simulink Block: Ideal Robot

The control strategy is decentralized, meaning each joint (J_1 to J_6) is governed by an independent control loop, as illustrated in Figure 16. This modular approach facilitates the tuning of individual gains for each actuator.

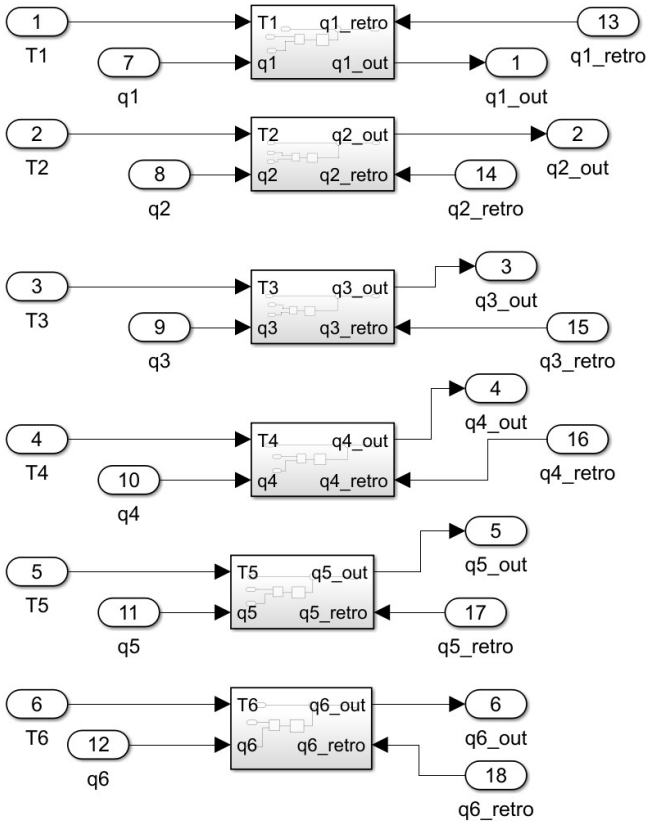

Figure 16. Simulink Block: Control loops for joints.

Specifically, a PD (Proportional-Derivative) controller with feedforward compensation is employed (Figure 17). This controller compares the desired position (q) against the feedback from the physical plant (q_retro) to compute the necessary torque (T), ensuring that the robotic arm executes precise angular corrections to maintain the tool within the required tolerance.

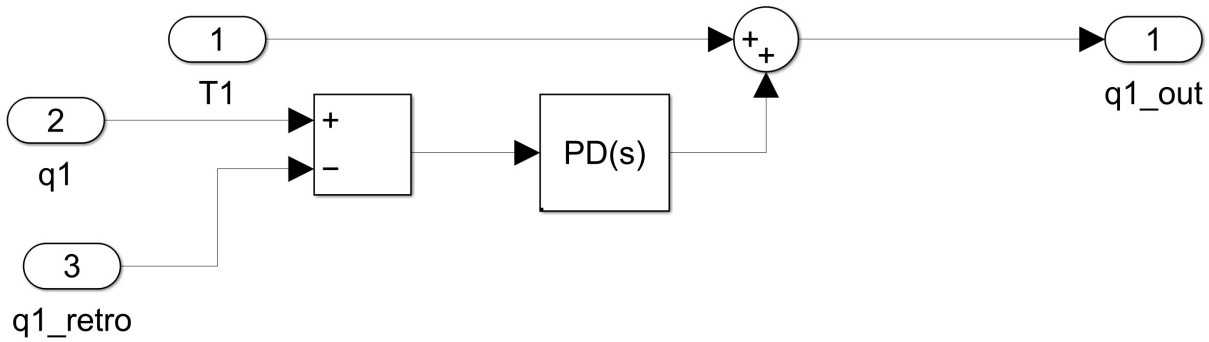

Figure 17. PD Controller + Feedforward Structure

This control structure implements a **Computed Torque Control** strategy with PD compensation architecture. Unlike a simple PID regulator, this system relies primarily on a dynamic feedforward term (τ_{ff}), calculated from the ideal inverse dynamics, which anticipates the torques required to overcome gravity, inertia, and Coriolis forces. The control law is defined as:

$$\tau_i = \tau_{ff,i} + K_{p,i} \cdot e_i + K_{d,i} \cdot \dot{e}_i \tag{2.1}$$

Where $K_{p,i}$ acts as a virtual stiffness and $K_{d,i}$ provides electronic damping.

It is important to note that, in this specific simulation, the feedforward model demonstrated high fidelity in predicting the required torque. Consequently, the proportional action (K_p) was sufficient to correct minor position errors, while the inherent mechanical damping modeled in the Simscape joints rendered high derivative gains unnecessary. This validates the accuracy of the mathematical model derived in the early stages, as the controller effectively operates by relying on the physics-based pre-calculation rather than reactive error correction.

Finally, to close the control loop, the physical behavior of the manipulator is simulated using the **Simscape Multibody** environment. Unlike simple kinematic animations, this block models the true dynamics of the system, assigning physical properties such as mass, center of gravity, and inertia tensors to each link. This setup allows for a rigorous assessment of whether the actuators possess sufficient torque to drive the 16 kg payload through the calculated trajectories, accounting for non-linear effects like gravity and joint friction.

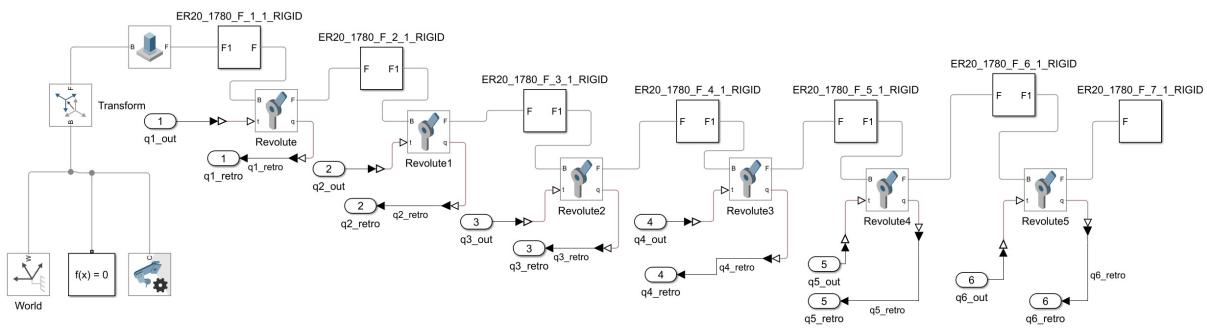

Figure 18. Simulink Block: Real Robot

The execution of the simulation in this virtual environment serves as a qualitative validation step. Visual inspection confirms that the manipulator successfully tracks the spatial coordinates defined in the input signal (*theta_simulink*), maintaining the tool orientation within the required welding constraints. The smooth motion observed, devoid of vibrations or kinematic singularities, corroborates the effectiveness of the feedforward-dominant control strategy and confirms the structural capability of the arm. This successful correlation between the mathematical generator and the physical simulator provides the necessary reliability to proceed with the quantitative analysis of the trajectory errors in the following stage.

2.3. STAGE III: SYSTEM VERIFICATION AND VALIDATION

2.3.1. Simulation and Validation

To perform the simulation and validate the movements of the predefined shapes, a code was used to generate a 3D animation of the robotic arm following trajectories calculated via iterative inverse kinematics. The model is defined symbolically using the Denavit–Hartenberg parameters from Table 1, and the homogeneous transformations of each link are converted into numerical functions for fast evaluation of joint configurations. An inverse kinematics method based on fsolve iteratively adjusts the joint values to reach the desired positions and orientations. The visualization module computes each joint's position and interpolates the trajectory points to display the motion frame by frame. This setup allows the robotic arm to execute the circular, square, and linear Z-axis trajectories accurately, as shown in Figures 19, 20, and 21.

- **Circular Trajectory:** is generated by interpolating three-dimensional points along a smooth curve within the chosen plane. Each point is sent to the inverse kinematics solver, which calculates the required joint configuration so that the end-effector maintains its orientation while following the curved path. As shown in Figure 19, this approach allows for assessing motion smoothness and stability of orientation throughout the trajectory. According to [8], such test scenarios are widely used to simulate complex processes like welding, enabling motion valida-

tion without the need for physical hardware.

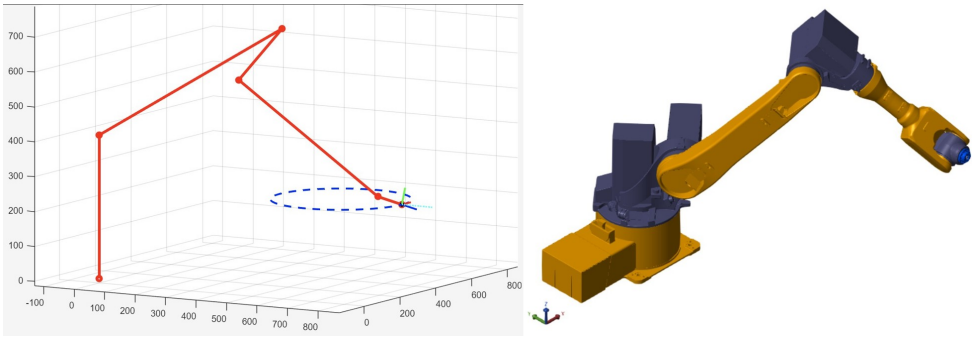

Figure 19. 3D Representation of Circular Motion.

- **Square Trajectory:**, the path is constructed from consecutive straight segments, each discretized into equally spaced points. The inverse kinematics solver computes each point to ensure the robot maintains consistent velocity, orientation, and smooth transitions at sharp corners. In Figure 20, the structured sequence of segments forming the square contour is shown, which is useful for analyzing corner stability. Precision evaluation through comparison with experimental data, as indicated in [4], allows validation of the geometric reliability of the generated motion.

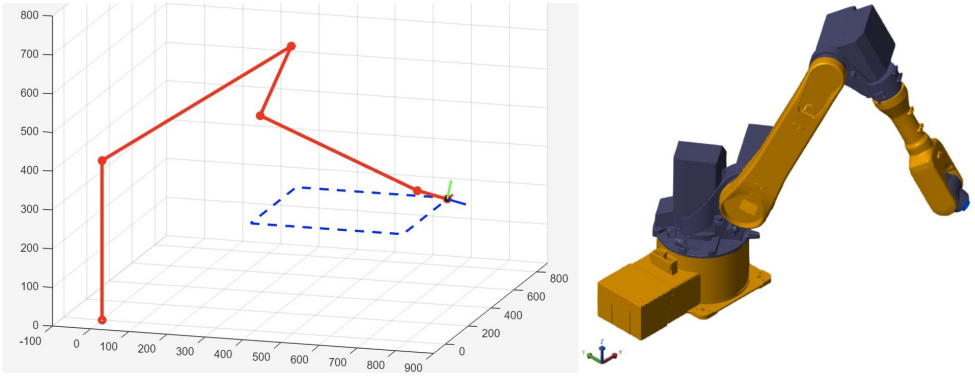

Figure 20. 3D Representation of Square Motion.

- **Linear Movement Along the Z-Axis:** is obtained by keeping X and Y fixed while Z varies uniformly, resulting in a pure vertical trajectory. Each point along the line is converted into a stable and aligned joint configuration, producing a straight displacement without lateral deviations. Figure 21 shows the straight path characteristic of this movement, ideal for analyzing axial stability. As studies like [24]

suggest, metrics such as mean squared error can quantify the precision of the end-effector tracking in this type of trajectory.

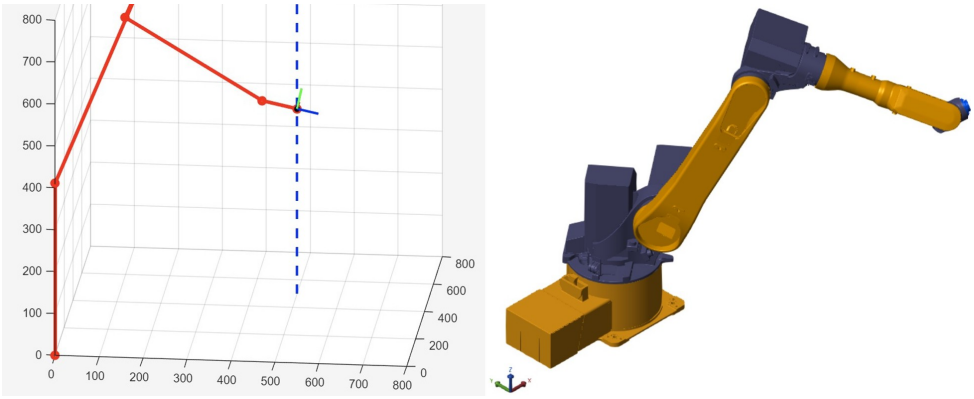

Figure 21. 3D Representation of Linear Movement Along the Z-Axis Motion.

2.3.2. Actuator Sizing Criteria and Service Factors

The selection of actuators involves applying a *Service Factor* (K_s) to the loads calculated under **Critical Operating Conditions**. These load values were validated through extensive dynamic simulations performed across two distinct operational workspaces to ensure reliability under different geometric configurations.

The specific simulation results supporting these values are detailed in the Appendices. Tables A.1, A.2, and A.3 present the torque measurements for Circular, Square, and Linear trajectories within *Workspace 1*, while Tables B.1, B.2, and B.3 detail the corresponding results for *Workspace 2*.

Based on the peak values observed in these simulations and mechanical design principles established in [29], the following safety factors were defined:

1. **Gravitational Axes (J2, J3, J5):** For joints primarily supporting static loads, a Safety Factor of $\mathbf{FS = 1.3}$ was selected. This aligns with industry recommendations to maintain the continuous RMS torque below 80% of the motor's rated capacity, preventing thermal overload during holding operations [30].

2. **Dynamic/Inertial Axes (J1, J4):** For the base (J1), which is subject to high start-up friction and inertial shock loads identified in the Workspace 1 simulations (Tables A.1-A.3), a conservative factor of $\mathbf{FS = 3.3}$ was applied. This margin is con-

sistent with AGMA standards for ”Heavy Shock” loads [31], ensuring the actuator can deliver the required peak torque (> 450 Nm) without saturation.

2.3.3. Analytical Torque Calculation Methodology

The required torque rating for the selected motor (τ_{motor}) is derived by applying the design safety factors to the calculated dynamic load (τ_{calc}), obtained via the Inverse Dynamics method. The governing equation is:

$$\tau_{motor} = \tau_{calc} \cdot FS = (\tau_{grav} + \tau_{inertial} + \tau_{friction}) \cdot FS \tag{2.2}$$

2.3.3.1. Wrist Unit Analysis (J4 – J6)

The wrist unit handles the direct manipulation of the welding torch.

- **Joint 6 (Hand):** The load is dominated by cable stiffness and friction rather than pure inertia.
- **Joint 5 (Doll):** Must overcome the gravitational torque of the offset torch in a cantilever configuration.
- **Joint 4 (Forearm Roll):** Subject to cross-inertial loads (gyroscopic effects) during rapid curved movements due to the 0.20 m tool offset.

2.3.3.2. Sample Calculation: Joint 2 (Shoulder)

To demonstrate the sizing methodology applied to the system, the specific calculation for Joint 2 is detailed below. This joint represents a critical case for gravitational holding torque.

1. **Determination of Calculated Load (τ_{calc}):** Based on the dynamic simulation of the kinematic chain (including link masses and the 10 kg payload), the peak torque required to maintain static equilibrium was determined to be:

$$\tau_{calc,J2} = 301.9\,\text{Nm}$$

2. **Application of Safety Factor (FS):** As established in the design criteria for gravitational axes, a factor of $FS = 1.3$ is applied [29].

3. **Calculation of Motor Torque Capacity (τ_{motor}):** Applying the design factor to the calculated load:

$$\tau_{motor,J2} = \tau_{calc,J2} \times FS$$

$$\tau_{motor,J2} = 301.9\,\text{Nm} \times 1.3 = 392.47\,\text{Nm}$$

Rounding for specification purposes:

$$\tau_{motor,J2} \approx 392.5\,\text{Nm}$$

Note: This identical calculation procedure was applied to all remaining degrees of freedom (J1, J3-J6) to determine the final actuator specifications.

2.3.4. Summary of Sizing Results

Table 2 summarizes the sizing results. The **Calculated Torque** column represents the physical load derived from the critical simulations, while the **Motor Torque** column indicates the minimum capacity required for the actuator selection.

Table 2. Actuator Sizing Requirements based on Critical Simulation Conditions

Joint	**Primary Load**	**Motor Torque** *(τ_{calc} [Nm])*	**Design Factor** *(FS)*	**Calculated Torque** **(τ_{motor} [Nm])**
J1 (Base)	Inertial	140.0	**3.3**	**462.0**
J2 (Shoulder)	Gravitational	301.9	1.3	**392.5**
J3 (Elbow)	Gravitational	129.3	1.3	**168.1**
J4 (Forearm)	Gyroscopic	25.1	3.0	**75.3**
J5 (Doll)	Gravitational	20.1	1.3	**26.1**
J6 (Hand)	Friction	2.6	1.5	**3.9**

Chapter 3

RESULTS

The simulation evaluated the robot's dynamic behavior across three representative trajectories: circular, square, and linear (Z-axis), utilizing the Denavit–Hartenberg parameters established in Table 1. To reflect real-world industrial scenarios based on standard [6], two operating modes were compared:

- **Continuous Mode (3.2 mm spacing):** Strictly constrained to a travel speed of **8 mm/s** to ensure adequate heat input and bead formation, simulating a thermally constrained welding process.
- **Intermittent Mode (40 mm spacing):** Allowed to utilize higher rapid-traverse speeds during non-welding transitions, simulating a rapid positioning task.

Performance metrics, including maximum torque peaks ($N \cdot m$) and trajectory tracking errors, were computed via MATLAB for all six joints (*J1–J6*) to identify critical stress points. While detailed datasets are provided in the Appendices, this section summarizes the critical findings.

3.1. CIRCULAR TRAJECTORY

To validate the circular trajectory, an experimental protocol was designed to adjust the radius (R) dynamically while adhering to the velocity constraints defined above. The analysis compares the high-precision continuous tracking required for a welding bead against the point-to-point motion used for spot welding or roughing.

3.1.1. Dynamic Torque Validation

To evaluate the dynamic demands placed on the actuators during the execution of the circular trajectory, the maximum torque (τ_{max}) was monitored at each of the six joints of the manipulator for the two working scenarios. The comparison of these results is

presented in Table 5, which contrasts the values obtained under the **Continuous configuration** (step of 3.2 mm) with those obtained under the **Intermittent configuration** (operating separation of 40 mm):

Table 3. Maximum Torque in Circular Trajectory: Continuous vs. Intermittent

No. (Test)	**Size** **(Radius)** [m]	**J1** **(Waist)** $[N \cdot m]$	**J2** **(Shoulder)** $[N \cdot m]$	**J3** **(Arm)** $[N \cdot m]$	**J4** **(Forearm)** $[N \cdot m]$	**J5** **(Doll)** $[N \cdot m]$	**J6** **(Hand)** $[N \cdot m]$
1	0.010	450 / 320	240 / 260	140 / 50	70 / 55	7.0 / 5.0	2.0 / 110
2	0.015	230 / 180	155 / 120	90 / 30	42 / 5	5.0 / 3.0	2.0 / 12
3	0.020	170 / 180	100 / 120	30 / 30	25 / 5	4.0 / 3.0	2.0 / 12
4	0.030	180 / 180	102 / 120	30 / 35	12 / 8	3.0 / 2.0	2.0 / 12
5	0.050	170 / 160	100 / 100	30 / 30	4 / 5	3.0 / 1.5	2.0 / 12
6	0.070	160 / 160	100 / 100	30 / 30	1.8 / 6	2.4 / 1.4	2.0 / 12
7	0.100	160 / 155	100 / 100	30 / 30	2 / 6	3.0 / 1.2	2.5 / 12
8	0.150	180 / 130	120 / 100	30 / 30	1.8 / 5	2.0 / 1.0	2.5 / 12
9	0.200	180 / 120	120 / 95	35 / 32	1.8 / 7	1.6 / 1.2	2.5 / 12
10	0.300	165 / 85	140 / 85	70 / 40	2.5 / 6	2.0 / 0.6	2.4 / 12

Note: Torque values are presented as: Continuous Mode / Intermittent Mode.

The analysis of the data shows that the **Continuous configuration** (3.2 mm) places a significantly higher mechanical load on the robot, especially during the initial movements where the base joint (J1) reached up to $450\ N \cdot m$, compared to the $320\ N \cdot m$ observed with the Intermittent strategy. Although the **Continuous Mode** operates at a lower velocity (6 mm/s), the requirement to strictly follow points that are very close together forces the manipulator to perform rapid and continuous micro-corrections to maintain path fidelity, increasing motor effort.

During larger circular trajectories, the main load shifts to joints J2 and J3 due to gravity; however, the intermittent mode remains more efficient by keeping overall dynamic demands lower. The only exception is the wrist joint (J6), which increases its torque to approximately $12\ N \cdot m$ (compared to $\sim\ 2\ N \cdot m$ in the **Continuous Mode**) due to the need to maintain a stiffer posture of the welding tool during the longer 40 mm displacements.

3.1.2. Evaluation of Trajectory Execution Accuracy

To validate the operational performance, the analysis focused on the positioning accuracy of the end-effector (Tool Center Point) by quantifying the error (E_p) as the Euclidean distance between the programmed target coordinates (P_{target}) and the actual coordinates (P_{actual}) in the 3D workspace. This metric captures the cumulative error of the kinematic chain, allowing for a direct assessment of spatial deviation magnitude as summarized in Table 6, which presents the maximum deviations observed under the most demanding test scenarios.

Table 4. Precision Error Distribution Across the 6 Joints (Test 4)

Joint	Mechanical Function	Error ($\%$) Cont. (3.2 mm)	Error ($\%$) Int. (40 mm)
J1	Waist (Rotation)	0.02%	0.16%
J2	Shoulder (Lift)	0.39%	0.11%
J3	Arm (Reach)	0.34%	0.67%
J4	Forearm Rotation	0.43%	1.06%
J5	Doll Rotation	**0.83%**	**2.89%**
J6	Hand (End-Effector)	0.18%	2.87%

The data clearly differentiates the behavior of the positioning joints (**J1–J3**) from that of the orientation joints (**J4–J6**). The joints responsible for placing the robot in X–Y–Z maintain stable accuracy in both strategies, typically staying below 0.5% error. Interestingly, **J2** performs slightly better under the intermittent strategy, likely due to reduced high-frequency vibrations that improve its control response.

In contrast, the orientation joints exhibit a significant loss of accuracy when the 40 mm spacing is applied. Both **J5** and **J6** reach error values close to 3%, showing that the intermittent strategy significantly increases the angular demand on the robot's wrist. This indicates that while overall positioning remains consistent, the end-effector orientation becomes more sensitive to dynamic variations and the higher angular accelerations required during longer steps.

3.2. CIRCULAR TRAJECTORY

To validate the circular trajectory, an experimental protocol was designed to adjust the radius (R) dynamically while adhering to the velocity constraints defined above. The analysis compares the high-precision continuous tracking required for a welding bead against the point-to-point motion used for spot welding or roughing. The complete experimental dataset comparing these scenarios corresponds to the results recorded in **Table A.1** (Workspace 1) and **Table B.1** (Workspace 2) of the Appendices.

3.2.1. Dynamic Torque Validation

To evaluate the dynamic demands placed on the actuators during the execution of the circular trajectory, the maximum torque (τ_{max}) was monitored at each of the six joints of the manipulator for the two working scenarios. The comparison of these results is presented in Table 5, which contrasts the values obtained under the **Continuous configuration** (step of 3.2 mm) with those obtained under the **Intermittent configuration** (operating separation of 40 mm).

Table 5. Maximum Torque in Circular Trajectory: Continuous vs. Intermittent

No. (Test)	Size (Radius) [m]	J1 (Waist) $[N \cdot m]$	J2 (Shoulder) $[N \cdot m]$	J3 (Arm) $[N \cdot m]$	J4 (Forearm) $[N \cdot m]$	J5 (Doll) $[N \cdot m]$	J6 (Hand) $[N \cdot m]$
1	0.010	450 / 320	240 / 260	140 / 50	70 / 55	7.0 / 5.0	2.0 / 110
2	0.015	230 / 180	155 / 120	90 / 30	42 / 5	5.0 / 3.0	2.0 / 12
3	0.020	170 / 180	100 / 120	30 / 30	25 / 5	4.0 / 3.0	2.0 / 12
4	0.030	180 / 180	102 / 120	30 / 35	12 / 8	3.0 / 2.0	2.0 / 12
5	0.050	170 / 160	100 / 100	30 / 30	4 / 5	3.0 / 1.5	2.0 / 12
6	0.070	160 / 160	100 / 100	30 / 30	1.8 / 6	2.4 / 1.4	2.0 / 12
7	0.100	160 / 155	100 / 100	30 / 30	2 / 6	3.0 / 1.2	2.5 / 12
8	0.150	180 / 130	120 / 100	30 / 30	1.8 / 5	2.0 / 1.0	2.5 / 12
9	0.200	180 / 120	120 / 95	35 / 32	1.8 / 7	1.6 / 1.2	2.5 / 12
10	0.300	165 / 85	140 / 85	70 / 40	2.5 / 6	2.0 / 0.6	2.4 / 12

Note: Torque values are presented as: Continuous Mode / Intermittent Mode.

The analysis indicates that the **Continuous configuration** (3.2 mm) imposes significantly higher mechanical loads, particularly on the base (J1), which peaked at $450\ N \cdot m$ versus $320\ N \cdot m$ in the Intermittent strategy. Despite the lower velocity (6 mm/s), the need for rapid micro-corrections to maintain path fidelity drives up motor effort. While

gravity dominates J2 and J3 loads in larger radii, the intermittent mode remains dynamically more efficient, except for the wrist (J6); here, torque rises to $\sim 12\ N \cdot m$ (vs. $\sim 2\ N \cdot m$) to stabilize the tool during the longer 40 mm displacements.

3.2.2. Evaluation of Trajectory Execution Accuracy

To validate the operational performance, the analysis focused on the positioning accuracy of the end-effector (Tool Center Point) by quantifying the error (E_p) as the Euclidean distance between the programmed target coordinates (P_{target}) and the actual coordinates (P_{actual}) in the 3D workspace. This metric captures the cumulative error of the kinematic chain, allowing for a direct assessment of spatial deviation magnitude as summarized in Table 6.

Table 6. Precision Error Distribution Across the 6 Joints (Test 4)

Joint	Mechanical Function	Error ($\%$) Cont. (3.2 mm)	Error ($\%$) Int. (40 mm)
J1	Waist (Rotation)	0.02%	0.16%
J2	Shoulder (Lift)	0.39%	0.11%
J3	Arm (Reach)	0.34%	0.67%
J4	Forearm Rotation	0.43%	1.06%
J5	Doll Rotation	**0.83%**	**2.89%**
J6	Hand (End-Effector)	0.18%	2.87%

The data clearly differentiates the behavior of the positioning joints (**J1–J3**) from that of the orientation joints (**J4–J6**). The joints responsible for placing the robot in X–Y–Z maintain stable accuracy in both strategies, typically staying below 0.5% error. Interestingly, **J2** performs slightly better under the intermittent strategy, likely due to reduced high-frequency vibrations that improve its control response. In contrast, the orientation joints exhibit a significant loss of accuracy when the 40 mm spacing is applied. Both **J5** and **J6** reach error values close to 3%, showing that the intermittent strategy significantly increases the angular demand on the robot's wrist.

3.3. SQUARE TRAJECTORY

The system's performance was evaluated using the **Side Length (L)** as the primary variable, comparing the **Continuous** strategy (3.2 mm) against the **Intermittent** strategy (40 mm) to analyze the robot's behavior at sharp 90° corners. A critical factor in this comparison is the velocity profile: while the **Continuous Mode** was constrained to a constant welding speed of 6 mm/s, the **Intermittent Mode** utilized rapid positioning speeds for the straight segments.

The complete experimental dataset comparing cycle times corresponds to the results recorded in **Table A.2** (Workspace 1) and **Table B.2** (Workspace 2) of the Appendices. The analysis of this data reveals that performance depends directly on geometry size. For small squares ($L = 0.045$ m), the difference is negligible as the inertial effort of corner braking dominates the cycle. However, for larger trajectories ($L = 0.400$ m), the intermittent strategy effectively exploits the long straight segments to accelerate beyond the process limit, achieving a **46% reduction in total cycle time** compared to the continuous mode.

3.3.1. Dynamic Torque Validation

The study of the Maximum Torque (τ_{max}) reveals a different behavior compared to the circular path: due to the geometry of the square, the robot must perform sharp decelerations when passing through each corner. As shown in Table 7, the **Intermittent** strategy (40 mm) imposes a significantly higher load on the robot's base joint (Joint 1), especially in medium and large trajectories. This indicates that long straight segments combined with 90° direction changes generate stronger inertial forces than those present in the smooth and constant 3.2 mm motion.

Table 7. Maximum Torque in Square Trajectory: Continuous vs. Intermittent

No. (Test)	**Side** **(m)**	**J1** **(Waist)** $[N \cdot m]$	**J2** **(Shoulder)** $[N \cdot m]$	**J3** **(Arm)** $[N \cdot m]$	**J4** **(Forearm)** $[N \cdot m]$	**J5** **(Doll)** $[N \cdot m]$	**J6** **(Hand)** $[N \cdot m]$
1	0.045	175 / 175	110 / 110	30 / 35	2 / 2	2 / 2	2 / 1
2	0.050	225 / 230	120 / 115	35 / 35	2 / 2	2 / 2	3 / 1
3	0.060	230 / 230	120 / 115	35 / 35	2 / 2	2 / 2	3 / 1
4	0.070	180 / **230**	120 / 115	35 / 35	2 / 2	2 / 2	3 / 1
5	0.095	240 / **300**	120 / 110	35 / 35	2 / 3	2 / 2	3 / 2
6	0.100	240 / **300**	120 / 110	35 / 35	2 / 3	2 / 2	3 / 2
7	0.150	240 / **300**	120 / 110	35 / 35	3 / 3	2 / 2	3 / 2
8	0.200	300 / **340**	100 / 100	35 / 75	3 / 3	2 / 2	3 / 2
9	0.300	270 / **340**	100 / 100	70 / 75	3 / 3	2 / 2	3 / 2
10	0.400	260 / **340**	**135** / **100**	**150** / **75**	3 / 3	6 / 2	3 / 2

Note: Torque values are presented as: Continuous Mode / Intermittent Mode.

The analysis reveals a clear trade-off in the robot's mechanical load: as the size of the square increases (from approximately 0.070 m onward), the intermittent strategy places significantly higher demand on the Base (J1), which must exert more force to stop and redirect the motion at each 90° corner; however, this added load brings a notable advantage to the rest of the arm, since the joints that carry most of the weight (J2 and J3) experience reduced stress, with the elbow torque dropping to nearly half in the largest test (Test 10).

3.3.2. Evaluation of Trajectory Execution Accuracy

Finally, the trajectory quality was assessed by examining the positioning error. Unlike the circular trajectory, where the main challenge was maintaining a constant curvature, the square trajectory demands stable linear motion along each side and accurate reorientation at every corner. The results reveal a clear functional split: the joints responsible for global positioning (J1, J2, and J3) preserve nearly identical stability across both strategies, while the wrist joint (J5) exhibits a noticeable improvement when using the intermittent method.

Table 8. Accuracy Error Distribution Across the 6 Joints

Joint	Mechanical Function	Error (%) Cont. (3.2 mm)	Error (%) Int. (40 mm)
J1	Waist (Rotation)	0.03%	0.02%
J2	Shoulder (Elevation)	0.03%	0.04%
J3	Arm (Reach)	0.10%	0.14%
J4	Forearm Rotation	0.00%	0.00%
J5	Doll Rotation	**2.40%**	**1.24%**
J6	Hand (End-Effector)	0.39%	0.13%

When evaluating the trajectory accuracy, the results are highly favorable for the intermittent strategy, particularly in the distal section of the robot. While the main axes (J1, J2, and J3) maintain impeccable precision in both scenarios, a substantial improvement is observed in the wrist assembly: both the orientation joint (J5) and the end-effector (J6) achieved significantly cleaner motion, reducing their errors drastically (J5 decreased by half and J6 dropped to a minimum of 0.13%), while J4 remained stable with practically negligible deviations.

3.4. LINEAR TRAJECTORY (Z-AXIS)

The behavior of the manipulator was examined during a purely vertical trajectory along the Z-axis, a physically demanding scenario where the robot works directly against gravitational force (g). The study compares the system's response when performing upward motions under the **Continuous** strategy (3.2 mm, physically constrained to 8 mm/s) versus the **Intermittent** strategy (40 mm, utilizing rapid traverse).

The complete experimental dataset comparing cycle times corresponds to the results recorded in **Table A.3** (Workspace 1) and **Table B.3** (Workspace 2) of the Appendices. In terms of speed, the intermittent approach maintains an advantage over longer distances precisely because it bypasses the process velocity limit imposed on the continuous mode. For short movements (< 0.4 m), the difference is slight; however, in the longest displacement (0.9 m), the intermittent strategy regains effectiveness, achieving a 13% reduction in total execution time by utilizing high-speed travel between points.

3.4.1. Dynamic Torque Validation

Unlike the square trajectory, where pauses give the arm brief relief, vertical movement behaves differently: **gravity penalizes stops**. Table 9 presents the maximum torques recorded under both strategies. It highlights how the joints responsible for elevation, particularly the Shoulder (J2), are significantly affected by the intermittent motion. Each stop every 40 mm causes the robot to lose upward momentum, forcing the joints to repeatedly overcome static friction and the weight of the arm.

Table 9. Maximum Torque in Vertical Trajectory: Continuous vs. Intermittent

No. (Test)	Height (m)	J1 (Waist) $[N \cdot m]$	J2 (Shoulder) $[N \cdot m]$	J3 (Arm) $[N \cdot m]$	J4 (Forearm) $[N \cdot m]$	J5 (Doll) $[N \cdot m]$	J6 (Hand) $[N \cdot m]$
1	0.05	380 / 400	325 / 300	105 / 98	4 / 4	5 / 6	1 / 1
2	0.10	380 / 400	300 / 300	95 / 98	4 / 4	5 / 6	1 / 1
3	0.20	380 / 380	275 / 275	85 / 90	3 / 4	5 / 5	1 / 1
4	0.30	365 / 365	240 / **300**	75 / **115**	4 / 4	5 / 5	1 / 1
5	0.40	340 / 350	265 / **340**	90 / **115**	3 / 4	5 / 5	1 / 1
6	0.50	330 / 310	270 / **360**	90 / **110**	3 / 4	4 / 5	1 / 1
7	0.60	270 / 230	265 / **360**	85 / **120**	3 / 3	3 / 5	1 / 1
8	0.70	230 / 230	290 / **360**	100 / **120**	2 / 3	4 / 5	1 / 1
9	0.80	190 / 180	290 / **350**	100 / **125**	2 / 3	4 / 5	1 / 1
10	0.90	150 / 170	270 / **320**	110 / **125**	2 / 3	4 / 5	1 / 1

Note: Torque values are presented as: Continuous Mode / Intermittent Mode.

The data clearly shows how the intermittent strategy significantly affects the joints responsible for elevation, particularly the Shoulder (J2) and Elbow (J3). As the robot stops every 40mm, it loses its accumulated upward momentum, forcing the joints to repeatedly overcome static friction and the arm's weight.

3.4.2. Evaluation of Trajectory Execution Accuracy

Positioning accuracy was evaluated, showing that stability is remarkably high for both strategies, with marginal errors rarely exceeding 1%. Table 10 demonstrates that there are no significant differences in the quality of the vertical trajectory. Both J5 (Wrist) and J6 (Flange) maintain consistent error levels, around 0.6% - 0.9%. This indicates that, although the intermittent strategy requires higher torque (energy), it does not compromise the geometric accuracy of the path.

Table 10. Distribution of Positioning Error Across the 6 Joints

Joint	Mechanical Function	Error (%) Cont. (3.2 mm)	Error (%) Int. (40 mm)
J1	Waist (Rotation)	0.03%	0.04%
J2	Shoulder (Elevation)	0.04%	0.04%
J3	Arm (Reach)	0.47%	0.48%
J4	Forearm Rotation	0.65%	0.59%
J5	Doll Rotation	**0.53%**	0.68%
J6	Hand (End-Effector)	0.95%	0.96%

In conclusion, for the vertical linear trajectory, the results reveal a trade-off: the intermittent strategy achieves a moderate time reduction (13%) thanks to rapid positioning speeds, but imposes a **substantial energy penalty** on the Shoulder and Elbow motors.

3.5. GENERAL MULTIVARIATE VALIDATION

This section integrates the results from the Circular, Square, and Linear trajectories. To rigorously validate the system, the analysis focuses on the **absolute maximum loads** experienced by the robot across all operational scenarios. This ”Worst-Case Scenario” approach ensures that the dynamic model and the selected actuators are capable of withstanding the highest stresses generated, regardless of the trajectory geometry.

3.5.1. Global Dynamic Validation: Worst-Case Analysis

Table 11 presents a comparison between the **Theoretical Torque** (calculated via Euler-Lagrange) and the **Maximum Simulated Torque** recorded during the entire experimental phase. The table highlights the highest stress peak recorded for each joint, regardless of which trajectory generated it, providing a safety margin validation for the motor selection.

Table 11. Global Validation: Maximum Torques Across All Trajectories

Joint	Calculated Torque (τ_{calc}) [$N \cdot m$]	Simulated Torque (τ_{sim}) [$N \cdot m$]	Relative Error [%]
J1	430.5	**450.0**	4.3%
J2	342.0	**360.0**	5.0%
J3	142.8	**150.0**	4.8%
J4	65.5	**70.0**	6.4%
J5	6.5	**7.0**	7.1%
J6	102.0	**110.0**	7.2%

3.5.2. Analysis of Critical Stress Points

The peak values presented above did not occur simultaneously; rather, they correspond to specific geometric conditions where the physical demands on each joint were maximized. The origin of these critical loads is detailed below:

- **Waist (J1):** The maximum torque of $450\ N \cdot m$ was recorded during the **Circular Trajectory**. This is attributed to the continuous change in the acceleration vector required to follow the curvature . Even at the constrained welding speed (6 mm/s), the high rotational inertia of the arm demands significant torque to maintain path fidelity during these constant directional updates.

- **Shoulder (J2):** The peak load of $360\ N \cdot m$ occurred during the **Vertical Linear Trajectory (Z-Axis)**. In this scenario, the motor must overcome the direct gravitational load to lift the entire arm structure from a standstill, without the aid of momentum.

- **Arm (J3):** The maximum stress of $150\ N \cdot m$ was observed in the **Square Trajectory**. This peak corresponds to the furthest corners of the square, where the lever arm is fully extended, maximizing the moment of force required to hold the forearm position.

- **Forearm, Doll and Hand (J4–J6):** The orientation joints experienced their highest demands during **Small-Radius Circular Trajectories**. The need for high-frequency corrections to maintain the welding torch orientation relative to the path resulted in instantaneous torque shocks, particularly in the end-effector (J6).

Despite the complexity of these varied scenarios, the error between the theoretical calculation and the simulation remains consistently below 8%. The slight increase in simulated torque is expected due to the inclusion of joint friction and complex inertia tensors in the CAD model, confirming that the dynamic model is robust and reliable for operational prediction.

Chapter 4

CONCLUSIONS AND RECOMMENDATIONS

4.1. CONCLUSIONS

- A robotic arm for automated welding was simulated in two working modes. In the main joints (J_1–J_3), both modes had errors below **0.5%**. However, the intermittent mode caused almost a 3% error in the wrist (J_4–J_6). Therefore, the continuous mode is the best choice for welding without deviations.

- The design and chosen motors proved to be highly resistant. They easily supported the maximum forces of **450 Nm** at the base (J_1) and **360 Nm** at the shoulder (J_2). The control system also kept the arm stable against gravity, making it ideal for the job.

- The geometric calculations used to guide the robot proved to be completely reliable. When testing different shapes, the parts responsible for positioning the arm (J_1–J_3) never lost track, always maintaining a minimal error below **0.5%**.

- Computer tests showed that the simulation is very realistic, with a difference of less than **8%** from the theory. When lifting the arm, the welding tool barely drifted off its path (less than **1%** error), confirming the prototype is accurate and reliable.

4.2. RECOMMENDATIONS

- Physical implementation of the project is recommended to validate critical real-world constraints, such as variable friction and thermal deformations, thereby evaluating factors that simulation does not fully account for.
- It is suggested that the model be evaluated with new trajectories and geometries to confirm its adaptability, thus ensuring that the prototype responds correctly to cases of work other than those already planned.
- To ensure the quality of the weld on the physical prototype, the use of high-precision gearboxes is recommended in order to avoid mechanical slack and vibrations, which could affect the stability of the arm and the final finish of the weld bead.

REFERENCES

[1] D. Akgümüs Gök, M. F. Özkan, H. E. Karaman, y M. S. M. Khattab, "Design and Kinematic Analysis of a Robotic Arm Capable of MIG Welding," *Osmaniye Korkut Ata Üniversitesi Fen Bilimleri Enstitüsü Dergisi*, vol. 8, no. 1, pp. 353–374, 2025.

[2] A. Sharma, R. Chaturvedi, K. Sharma, S. Abrahim Binhowimal, J. Giri, y T. Sathish, "Enhancing weld quality of novel robotic-arm arc welding: Vision-based monitoring, real-time control seam tracking," *Ain Shams Engineering Journal*, vol. 15, no. 12, p. 103109, 2024.

[3] American Welding Society, *AWS D1.1/D1.1M:2020 Structural Welding Code – Steel*, American Welding Society, Miami, FL, 2020, 24th Edition.

[4] A. N. Huda, D. Pebrianti, y Z. Zain, "Integrated Robotic Arm Control: Inverse Kinematics, Trajectory Planning, and Performance Evaluation for Automated Welding," *Asian Journal Science and Engineering*, vol. 2, no. 2, 2023.

[5] L. Armas, J. N. Castillo, y L. O. Freire, "Simulación y modelamiento matemático de un brazo robótico de 4 grados de libertad," *Ciencias De La Ingeniería Y Aplicadas*, vol. 9, no. 2, pp. 144–156, 2025.

[6] S. de Comunicaciones y Transportes (SCT) de México, "Libro: Cmt. características de los materiales. parte 2. materiales para estructuras. título 04. soldadura. capítulo 001. soldadura al arco eléctrico," Norma N·CMT·2·04·001/04, disponible en línea, 2004, 15 diciembre 2004. [En línea]. Disponible: https://normas.imt.mx/storage/normativa/N-CMT-2-04-001-04.pdf

[7] A. Torres, "Control of a teleoperated 6-degree-of-freedom anthropomorphic robotic arm for industrial safety in Peru," *Perfiles de Ingeniería*, vol. 2, no. 11, pp. 31–41, 2020.

[8] Y. Smirnov, A. Kalyashina, y R. Zaripova, “Simulation of Robotic Laser Welding Process,” in *2022 International Russian Automation Conference (RusAutoCon)*, 2022, pp. 1–5.

[9] D. Suquilanda, N. M. Suárez Figueroa, y A. A. Mora Figueroa, “Advanced simulation of a 2-degree-of-freedom robotic arm controlled in Simscape,” *Ecosur*, vol. 1, no. 06, pp. 22–40, 2024.

[10] D. N. Cuesta Cuesta y J. R. Garavito Martinez, “Design and construction of a 6 DOF robotic arm for educational purposes,” sin especificar.

[11] J. K. Millán Castrillón, “Programmed motion system for a 6-degree-of-freedom miniature robotic arm,” Tesis de maestría, Unspecified, 2019.

[12] C. J. Fuentes Flores y H. E. Zunini Vasquez, “Design of a 6-degree-of-freedom robotic arm for painting blades at AYNI SAC-La Libertad,” Tesis de maestría, Unspecified, 2019.

[13] D. A. Robles Nieto, T. A. Díaz Carrillo, y J. Rueda Mayorga, “Design, construction and control of a 6-degree-of-freedom anthropomorphic robotic arm and a 4-degree-of-freedom SCARA robotic arm,” 2015.

[14] A. F. Araque Mora y F. J. Pedroza Fernández, “Development of a 6-degree-of-freedom manipulator robot with open technologies,” in *Unspecified*, 2019.

[15] G. N. Montenegro Alcívar y M. L. Yaguachi Ríos, “Design, construction and control of a prototype anthropomorphic robotic arm for spot welding different shapes, using inverse kinematics and artificial vision,” Tesis de maestría, Unspecified, 2020.

[16] L. E. Flores Torres, “Design of a robotic arm with an angular configuration and 6 degrees of freedom with a reach of one meter intended for electric arc welding processes with linear trajectories,” Tesis de maestría, Unspecified, 2015.

[17] Google DeepMind, “Gemini (Large Language Model),” https://gemini.google.com/, 2024, imagen generada mediante inteligencia artificial a partir de bocetos del autor.

[18] D. A. Jaramillo Rojas, “Modelo, simulación y control de un brazo robótico mediante matlab y simulink para soldadura de arco,” Tesis de maestría, EPN, QUITO, 2010.

[19] A. N. Barakat, K. A. Gouda, y K. A. Bozed, “Kinematics analysis and simulation of a robotic arm using MATLAB,” in *2016 4th International Conference on Control Engineering & Information Technology (CEIT)*, 2016, pp. 1–5.

[20] W. G. Salazar Patín, “Design of a user interface and kinematic control of a 6-degree-of-freedom robotic arm for trajectory planning in Matlab and Simulink software,” Tesis de maestría, Unspecified, 2015.

[21] I. A. R. R., “Modelling and Simulation of a 6-DOF Industrial Robot with a Universal Robot Language on a PC-Based Virtual Controller,” *Advances in Robotics*, vol. 5, no. 1, pp. 83–89, 2018.

[22] J. W. e. a. K., “Kinematic Analysis and Trajectory Planning of 6-DOF Industrial Robot based on CATIA and MATLAB Simulation,” in *MATEC Web of Conferences*, vol. 153, 2018.

[23] P. I. Corke, “A Robotics Toolbox for MATLAB,” *IEEE Robotics and Automation Magazine*, vol. 3, no. 1, pp. 24–32, 1996.

[24] B. E. Nyong-Bassey y A. M. Epemu, “Inverse Kinematics Analysis of Novel 6-DOF Robotic Arm Manipulator for Oil and Gas Welding Using Meta-Heuristic Algorithms,” *International Journal on Robotics, Automation and Sciences*, vol. 4, no. 3, pp. 13–22, 2022.

[25] Inspenet. Soldadura mig en procesos de fabricación. [En línea]. Disponible: https://inspenet.com/articulo/soldadura-mig-en-procesos-de-fabricacion/ (2023) Accessed: 2025-11-21.

[26] W. Commons. Gmaw weld area. [En línea]. Disponible: https://commons.wikimedia.org/wiki/File:GMAW-weld-area.png (n.d.) Accessed: 2025-12-07.

[27] R. Munir, R. C. Alfi, y H. Junaidi, “Implementasi Pergerakan Robot Lengan 4 Derajat Kebebasan Menggunakan Kendali Proporsional Integral Derivative (PID),” *Jurnal Robotika dan Otomasi*, vol. 1, no. 1, pp. 24–29, 2021.

[28] R. M. A. W. C. L. A. S., “Sistem Pengontrolan Robot Lengan Untuk Mengikuti Bentuk Objek Pada Aplikasi Painting,” *Jurnal ELK-Kom*, vol. 2, no. 1, pp. 19–24, 2019.

[29] R. G. Budynas y J. K. Nisbett, *Shigley’s Mechanical Engineering Design*, 11th ed. McGraw-Hill Education, 2020, chapter 1: Design Factors and Safety Factors.

[30] Yaskawa America Inc., *Sigma-7 Series Servo Systems: Sizing and Selection Guide*, Yaskawa, 2019, technical Reference SIGMA-7-SIZING. [En línea]. Disponible: https://www.yaskawa.com

[31] American Gear Manufacturers Association, “Fundamental rating factors and calculation methods for involute spur and helical gear teeth,” AGMA, Tech. Rep. ANSI/AGMA 2001-D04, 2004.

APPENDIX A

RESULTS DATA

TABLE A.1

Simulation results for the Circular (Workspace 1).

AREA DE TRABAJO 1																	
SEPARACION DE 3,2 MM POR NORMA (CONTINUO)									SEPARACION DE 40 MM POR NORMA (CON INTERMITENCIA)								
NUMERO DE PRUEBA CONTINUO	VELOCIDAD (mm/s)	JUNTAS	CIRCULO						NUMERO DE PRUEBA INTERMITENTE	VELOCIDAD (mm/s)	JUNTAS	CIRCULO					
			RADIO (mm)	TIEMPO (s)		TORQUE MAXIMO (N*m)	ERROR	OBSERVACIONES				RADIO (mm)	TIEMPO (s)		TORQUE MAXIMO (N*m)	ERROR	OBSERVACIONES
				TRAYECTORIA	FINAL								TRAYECTORIA	FINAL			
1	8	J1	10	10,42	55,47	450	99,976	TIENE UN ERROR DEL 2%	1	6	J1	10	10,43	41,43	320	99,976	
		J2				240	99,969				J2				260	99,969	
		J3				140	99,706				J3				50	99,706	
		J4				70	99,991				J4				55	98,991	
		J5				7	98,385				J5				5	98,385	
		J6				2	99,616				J6				110	99,616	
2	8	J1	15	11,48	61,48	230	99,976	TIENE UN ERROR DEL 2%	2	8	J1	15	11,76	52,76	180	99,975	TIENE UN ERROR DEL 2%
		J2				155	99,966				J2				120	99,966	
		J3				90	99,695				J3				30	99,964	
		J4				42	99,043				J4				5	99,036	
		J5				5	98,151				J5				3	98,029	
		J6				2	99,631				J6				12	99,623	
3	8	J1	20	20,92	61,92	170	99,977		3	8	J1	20	15,70	56,70	180	99,978	
		J2				100	99,964				J2				120	99,967	
		J3				30	99,673				J3				30	99,719	
		J4				25	99,228				J4				5	99,266	
		J5				4	98,853				J5				3	99,095	
		J6				2	99,752				J6				12	99,699	
4	8	J1	30	31,40	72,40	180	99,975		4	8	J1	30	23,55	64,55	180	99,835	TIENE UN ERROR DEL 2% Y HASTA EL 3%
		J2				102	99,61				J2				120	99,891	
		J3				30	99,659				J3				35	99,331	
		J4				12	99,567				J4				8	98,938	
		J5				3	99,166				J5				2	97,11	
		J6				2	99,815				J6				12	97,127	
5	8	J1	50	52,35	93,35	170	99,979		5	10	J1	50	30,61	71,61	160	99,932	TIENE UN ERROR DEL 2%
		J2				100	99,975				J2				100	99,932	
		J3				30	99,308				J3				30	99,575	
		J4				4	99,267				J4				5	99,42	
		J5				3	99,476				J5				1,5	98,498	
		J6				2	99,677				J6				12	98,041	
6	8	J1	70	73,29	114,29	160	99,977		6	10	J1	70	43,38	84,38	160	99,983	
		J2				100	99,975				J2				100	99,979	
		J3				30	99,736				J3				30	99,78	
		J4				1,8	99,691				J4				6	99,52	
		J5				2,4	99,66				J5				1,4	99,446	
		J6				2	99,82				J6				12	99,77	
7	8	J1	100	104,71	145,71	160	99,985		7	10	J1	100	62,42	103,43	155	99,982	
		J2				100	99,979				J2				100	99,977	
		J3				30	99,772				J3				30	99,778	
		J4				2	99,431				J4				6	99,428	
		J5				3	99,204				J5				1,2	99,683	
		J6				2,5	99,665				J6				12	99,864	
8	8	J1	150	157,07	198,07	180	99,983		8	12	J1	150	78,31	119,31	130	99,982	
		J2				120	99,979				J2				100	99,978	
		J3				30	99,826				J3				30	99,835	
		J4				1,8	99,297				J4				5,2	99,413	
		J5				2	99,408				J5				1	99,734	
		J6				2,5	99,781				J6				12	99,895	
9	8	J1	200	209,43	250,43	180	99,982		9	12	J1	200	104,55	145,55	120	99,983	
		J2				120	99,975				J2				95	99,98	
		J3				35	99,86				J3				32	99,878	
		J4				1,8	99,424				J4				7	99,417	
		J5				1,6	99,683				J5				1,2	99,591	
		J6				2,5	99,856				J6				12	99,883	
10	8	J1	300	314,15	355,15	165	99,988		10	12	J1	300	157,07	198,07	85	99,988	
		J2				140	99,978				J2				85	99,78	
		J3				70	99,925				J3				40	99,925	
		J4				2,5	99,956				J4				6	99,955	
		J5				2	99,489				J5				0.6	99,49	
		J6				2,4	99,849				J6				12	99,872	

TABLE A.2

Simulation results for the Square trajectory (Workspace 1).

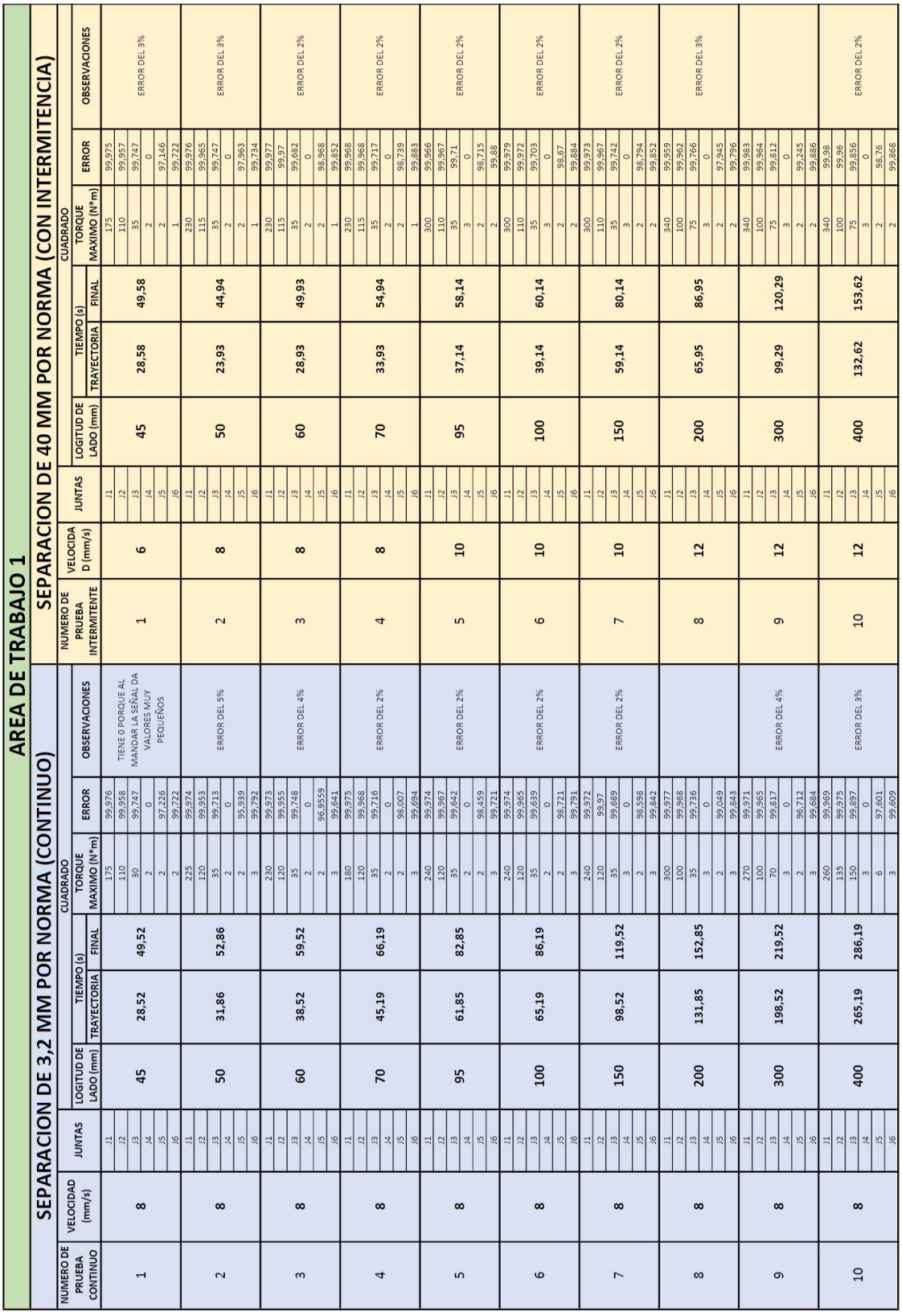

AREA DE TRABAJO 1

SEPARACION DE 3,2 MM POR NORMA (CONTINUO)

NUMERO DE PRUEBA CONTINUO	VELOCIDAD (mm/s)	JUNTAS	CUADRADO						OBSERVACIONES
			LOGITUD DE LADO (mm)	TIEMPO (s)		TORQUE MAXIMO (N*m)	ERROR		
				TRAYECTORIA	FINAL				
1	8	J1	45	28,52	49,52	175	99,976	TIENE 0 PORQUE AL MANDAR LA SEÑAL DA VALORES MUY PEQUEÑOS	
		J2				110	99,958		
		J3				30	99,747		
		J4				2	0		
		J5				2	97,226		
		J6				2	99,722		
2	8	J1	50	31,86	52,86	225	99,974	ERROR DEL 5%	
		J2				120	99,953		
		J3				35	99,713		
		J4				2	0		
		J5				2	95,939		
		J6				3	99,792		
3	8	J1	60	38,52	59,52	230	99,973	ERROR DEL 4%	
		J2				120	99,955		
		J3				35	99,748		
		J4				2	0		
		J5				2	96,9559		
		J6				3	99,641		
4	8	J1	70	45,19	66,19	180	99,975	ERROR DEL 2%	
		J2				120	99,968		
		J3				35	99,716		
		J4				2	0		
		J5				2	98,007		
		J6				3	99,694		
5	8	J1	95	61,85	82,85	240	99,974	ERROR DEL 2%	
		J2				120	99,967		
		J3				35	99,642		
		J4				2	0		
		J5				2	98,459		
		J6				3	99,721		
6	8	J1	100	65,19	86,19	240	99,974	ERROR DEL 2%	
		J2				120	99,965		
		J3				35	99,639		
		J4				2	0		
		J5				2	98,721		
		J6				3	99,791		
7	8	J1	150	98,52	119,52	240	99,972	ERROR DEL 2%	
		J2				120	99,97		
		J3				35	99,689		
		J4				3	0		
		J5				2	98,598		
		J6				3	99,842		
8	8	J1	200	131,85	152,85	300	99,977		
		J2				100	99,968		
		J3				35	99,736		
		J4				3	0		
		J5				2	99,049		
		J6				3	99,843		
9	8	J1	300	198,52	219,52	270	99,971	ERROR DEL 4%	
		J2				100	99,965		
		J3				70	99,817		
		J4				3	0		
		J5				2	96,712		
		J6				3	99,684		
10	8	J1	400	265,19	286,19	260	99,969	ERROR DEL 3%	
		J2				135	99,975		
		J3				150	99,897		
		J4				3	0		
		J5				6	97,601		
		J6				3	99,609		

SEPARACION DE 40 MM POR NORMA (CON INTERMITENCIA)

NUMERO DE PRUEBA INTERMITENTE	VELOCIDAD (mm/s)	JUNTAS	CUADRADO					OBSERVACIONES
			LOGITUD DE LADO (mm)	TIEMPO (s)		TORQUE MAXIMO (N*m)	ERROR	
				TRAYECTORIA	FINAL			
1	6	J1	45	28,58	49,58	175	99,975	ERROR DEL 3%
		J2				110	99,957	
		J3				35	99,747	
		J4				2	0	
		J5				2	97,146	
		J6				1	99,722	
2	8	J1	50	23,93	44,94	230	99,976	ERROR DEL 3%
		J2				115	99,965	
		J3				35	99,747	
		J4				2	0	
		J5				2	97,963	
		J6				1	99,734	
3	8	J1	60	28,93	49,93	230	99,977	ERROR DEL 2%
		J2				115	99,97	
		J3				35	99,682	
		J4				2	0	
		J5				2	98,968	
		J6				1	99,852	
4	8	J1	70	33,93	54,94	230	99,968	ERROR DEL 2%
		J2				115	99,968	
		J3				35	99,717	
		J4				2	0	
		J5				2	98,739	
		J6				1	99,883	
5	8	J1	95	37,14	58,14	300	99,966	ERROR DEL 2%
		J2				110	99,967	
		J3				35	99,71	
		J4				3	0	
		J5				2	98,715	
		J6				2	99,88	
6	8	J1	100	39,14	60,14	300	99,979	ERROR DEL 2%
		J2				110	99,972	
		J3				35	99,703	
		J4				3	0	
		J5				2	98,67	
		J6				2	99,884	
7	8	J1	150	59,14	80,14	300	99,973	ERROR DEL 2%
		J2				110	99,967	
		J3				35	99,742	
		J4				3	0	
		J5				2	98,794	
		J6				2	99,852	
8	8	J1	200	65,95	86,95	340	99,959	ERROR DEL 3%
		J2				100	99,962	
		J3				75	99,766	
		J4				3	0	
		J5				2	97,945	
		J6				2	99,796	
9	8	J1	300	99,29	120,29	340	99,983	
		J2				100	99,964	
		J3				75	99,812	
		J4				3	0	
		J5				2	99,245	
		J6				2	99,886	
10	8	J1	400	132,62	153,62	340	99,98	ERROR DEL 2%
		J2				100	99,96	
		J3				75	99,856	
		J4				3	0	
		J5				2	98,76	
		J6				2	99,868	

TABLE A.3

Simulation results for the Linear trajectory (Workspace 1).

AREA DE TRABAJO 1

SEPARACION DE 3,2 MM POR NORMA (CONTINUO)

NUMERO DE PRUEBA CONTINUO	VELOCIDAD (mm/s)	JUNTAS	LINEA RECTA EN EL EJE Z					
			TAMAÑO (mm)	TIEMPO (s)		TORQUE MAXIMO (N*m)	ERROR	OBSERVACIONES
				TRAYECTORIA	FINAL			
1	8	J1	50	8,33	16,33	380	99,904	ERROR DEL 5%
		J2				325	99,909	
		J3				105	99,427	
		J4				4	95,944	
		J5				5	99,098	
		J6				1	99,007	
2	8	J1	100	12,50	20,50	380	99,63	ERROR DEL 2%
		J2				300	99,936	
		J3				95	99,09	
		J4				4	98,571	
		J5				5	99,677	
		J6				1	99,636	
3	8	J1	200	25,00	33,00	380	99,956	
		J2				275	99,95	
		J3				85	99,205	
		J4				3	99,202	
		J5				5	99,73	
		J6				1	99,398	
4	8	J1	300	37,50	45,50	365	99,959	
		J2				240	99,956	
		J3				75	99,389	
		J4				4	99,152	
		J5				5	99,584	
		J6				1	99,297	
5	8	J1	400	40,00	48,00	340	99,966	
		J2				265	99,961	
		J3				90	99,58	
		J4				3	99,122	
		J5				5	99,324	
		J6				1	99,225	
6	8	J1	500	41,66	49,66	330	99,965	
		J2				270	99,96	
		J3				90	99,55	
		J4				3	99,26	
		J5				4	99,557	
		J6				1	99,192	
7	8	J1	600	50,00	58,00	270	99,965	
		J2				265	99,96	
		J3				85	99,589	
		J4				3	99,212	
		J5				3	99,319	
		J6				1	99,208	
8	8	J1	700	58,33	66,33	230	99,965	
		J2				290	99,959	
		J3				100	99,542	
		J4				2	99,33	
		J5				4	99,565	
		J6				1	99,137	
9	8	J1	800	66,66	74,66	190	99,969	
		J2				290	99,962	
		J3				100	99,535	
		J4				2	99,34	
		J5				4	99,35	
		J6				1	99,143	
10	8	J1	900	75	83	150	99,968	
		J2				270	99,96	
		J3				110	99,526	
		J4				2	99,355	
		J5				4	99,47	
		J6				1	99,055	

SEPARACION DE 40 MM POR NORMA (CON INTERMITENCIA)

NUMERO DE PRUEBA INTERMITENTE	VELOCIDAD (mm/s)	JUNTAS	LINEA RECTA EN EL EJE Z					
			TAMAÑO (mm)	TIEMPO (s)		TORQUE MAXIMO (N*m)	ERROR	OBSERVACIONES
				TRAYECTORIA	FINAL			
1	6	J1	50	6,25	14,25	400	99,892	ERROR DEL 6%
		J2				300	99,891	
		J3				98	99,129	
		J4				4	94,925	
		J5				6	98,911	
		J6				1	98,666	
2	8	J1	100	10,00	18,00	400	99,917	
		J2				300	99,924	
		J3				98	99,429	
		J4				4	99,131	
		J5				6	99,556	
		J6				1	99,344	
3	8	J1	200	20,00	28,00	380	99,953	ERROR DEL 2%
		J2				275	99,946	
		J3				90	98,929	
		J4				4	99,132	
		J5				5	99,689	
		J6				1	99,568	
4	8	J1	300	30,00	38,00	365	99,954	
		J2				300	99,949	
		J3				115	99,364	
		J4				4	99,098	
		J5				5	99,742	
		J6				1	99,226	
5	10	J1	400	36,36	44,36	350	99,958	
		J2				340	99,955	
		J3				115	99,481	
		J4				4	99,209	
		J5				5	99,54	
		J6				1	99,276	
6	10	J1	500	45,45	53,45	310	99,963	
		J2				360	99,958	
		J3				110	99,522	
		J4				4	99,078	
		J5				5	98,932	
		J6				1	99,219	
7	10	J1	600	54,54	62,54	230	99,965	
		J2				360	99,959	
		J3				120	99,591	
		J4				3	99,311	
		J5				5	99,315	
		J6				1	99,188	
8	12	J1	700	50,00	58,00	230	99,65	
		J2				360	99,958	
		J3				120	99,573	
		J4				3	99,313	
		J5				5	99,382	
		J6				1	99,155	
9	12	J1	800	57,14	65,14	180	99,965	
		J2				350	99,958	
		J3				125	99,541	
		J4				3	99,416	
		J5				5	99,584	
		J6				1	99,088	
10	12	J1	900	64,28	72,28	170	99,965	
		J2				320	99,957	
		J3				125	99,524	
		J4				3	99,415	
		J5				5	99,319	
		J6				1	99,038	

TABLE B.1

Simulation results for the Circular trajectory (Workspace 2).

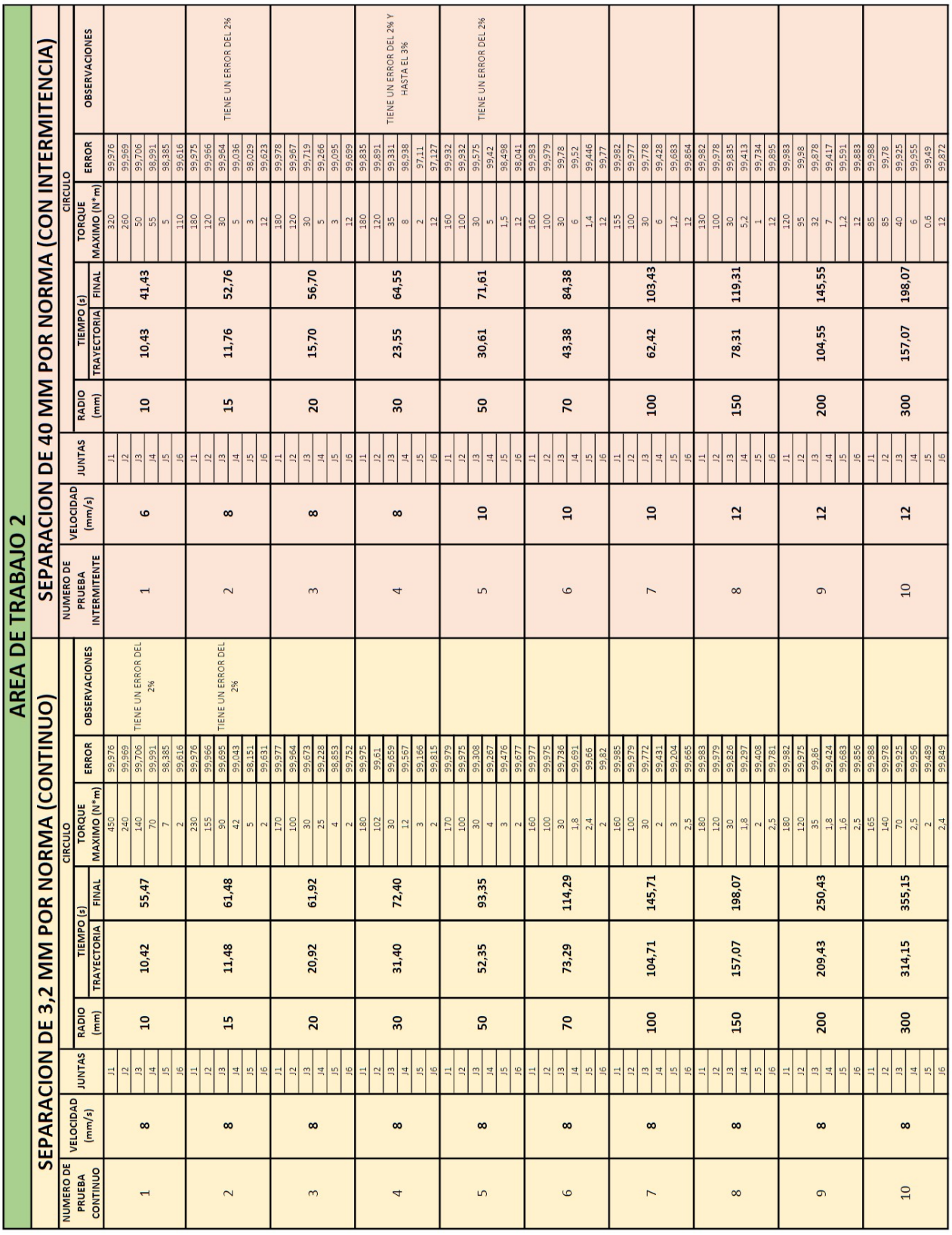

AREA DE TRABAJO 2

NUMERO DE PRUEBA CONTINUO	VELOCIDAD (mm/s)	JUNTAS	SEPARACION DE 3,2 MM POR NORMA (CONTINUO) RADIO (mm)	TIEMPO (s) TRAYECTORIA	TIEMPO (s) FINAL	CIRCULO TORQUE MAXIMO (N*m)	CIRCULO ERROR	OBSERVACIONES	NUMERO DE PRUEBA INTERMITENTE	VELOCIDAD (mm/s)	JUNTAS	SEPARACION DE 40 MM POR NORMA (CON INTERMITENCIA) RADIO (mm)	TIEMPO (s) TRAYECTORIA	TIEMPO (s) FINAL	CIRCULO TORQUE MAXIMO (N*m)	CIRCULO ERROR	OBSERVACIONES
1	8	J1	10	10,42	55,47	450	99,976	TIENE UN ERROR DEL 2%	1	6	J1	10	10,43	41,43	320	99,976	
		J2				240	99,969				J2				260	99,969	
		J3				140	99,706				J3				50	99,706	
		J4				70	99,991				J4				55	98,991	
		J5				7	98,385				J5				5	98,385	
		J6				2	99,616				J6				110	99,616	
2	8	J1	15	11,48	61,48	230	99,976	TIENE UN ERROR DEL 2%	2	8	J1	15	11,76	52,76	180	99,975	TIENE UN ERROR DEL 2%
		J2				155	99,966				J2				120	99,966	
		J3				90	99,695				J3				30	99,964	
		J4				42	99,043				J4				5	99,036	
		J5				5	98,151				J5				3	98,029	
		J6				2	99,631				J6				12	99,623	
3	8	J1	20	20,92	61,92	170	99,977		3	8	J1	20	15,70	56,70	180	99,978	
		J2				100	99,964				J2				120	99,967	
		J3				30	99,673				J3				30	99,719	
		J4				25	99,228				J4				5	99,266	
		J5				4	98,853				J5				3	99,095	
		J6				2	99,752				J6				12	99,699	
4	8	J1	30	31,40	72,40	180	99,975		4	8	J1	30	23,55	64,55	180	99,835	TIENE UN ERROR DEL 2% Y HASTA EL 3%
		J2				102	99,61				J2				120	99,891	
		J3				30	99,659				J3				35	99,331	
		J4				12	99,567				J4				8	98,938	
		J5				3	99,166				J5				2	97,11	
		J6				2	98,815				J6				12	97,127	
5	8	J1	50	52,35	93,35	170	99,979		5	10	J1	50	30,61	71,61	160	99,932	TIENE UN ERROR DEL 2%
		J2				100	99,975				J2				100	99,932	
		J3				30	99,308				J3				30	99,575	
		J4				4	99,267				J4				5	99,42	
		J5				3	99,476				J5				1,5	98,498	
		J6				2	99,677				J6				12	98,041	
6	8	J1	70	73,29	114,29	160	99,977		6	10	J1	70	43,38	84,38	160	99,983	
		J2				100	99,975				J2				100	99,979	
		J3				30	99,736				J3				30	99,78	
		J4				1,8	99,691				J4				6	99,52	
		J5				2,4	99,66				J5				1,4	99,446	
		J6				2	99,82				J6				12	99,77	
7	8	J1	100	104,71	145,71	160	99,985		7	10	J1	100	62,42	103,43	155	99,982	
		J2				100	99,979				J2				100	99,977	
		J3				30	99,772				J3				30	99,778	
		J4				2	99,431				J4				6	99,428	
		J5				3	99,204				J5				1,2	99,683	
		J6				2,5	99,665				J6				12	99,864	
8	8	J1	150	157,07	198,07	180	99,983		8	12	J1	150	78,31	119,31	130	99,982	
		J2				120	99,979				J2				100	99,978	
		J3				30	99,826				J3				30	99,835	
		J4				1,8	99,297				J4				5,2	99,413	
		J5				2	99,408				J5				1	99,734	
		J6				2,5	99,781				J6				12	99,895	
9	8	J1	200	209,43	250,43	180	99,982		9	12	J1	200	104,55	145,55	120	99,983	
		J2				120	99,975				J2				95	99,98	
		J3				35	99,86				J3				32	99,878	
		J4				1,8	99,424				J4				7	99,417	
		J5				1,6	99,683				J5				1,2	99,591	
		J6				2,5	99,856				J6				12	99,883	
10	8	J1	300	314,15	355,15	165	99,988		10	12	J1	300	157,07	198,07	85	99,988	
		J2				140	99,978				J2				85	99,78	
		J3				70	99,925				J3				40	99,925	
		J4				2,5	99,956				J4				6	99,955	
		J5				2	99,489				J5				0,6	99,49	
		J6				2,4	99,849				J6				12	99,872	

TABLE B.2

Simulation results for the Square trajectory (Workspace 2).

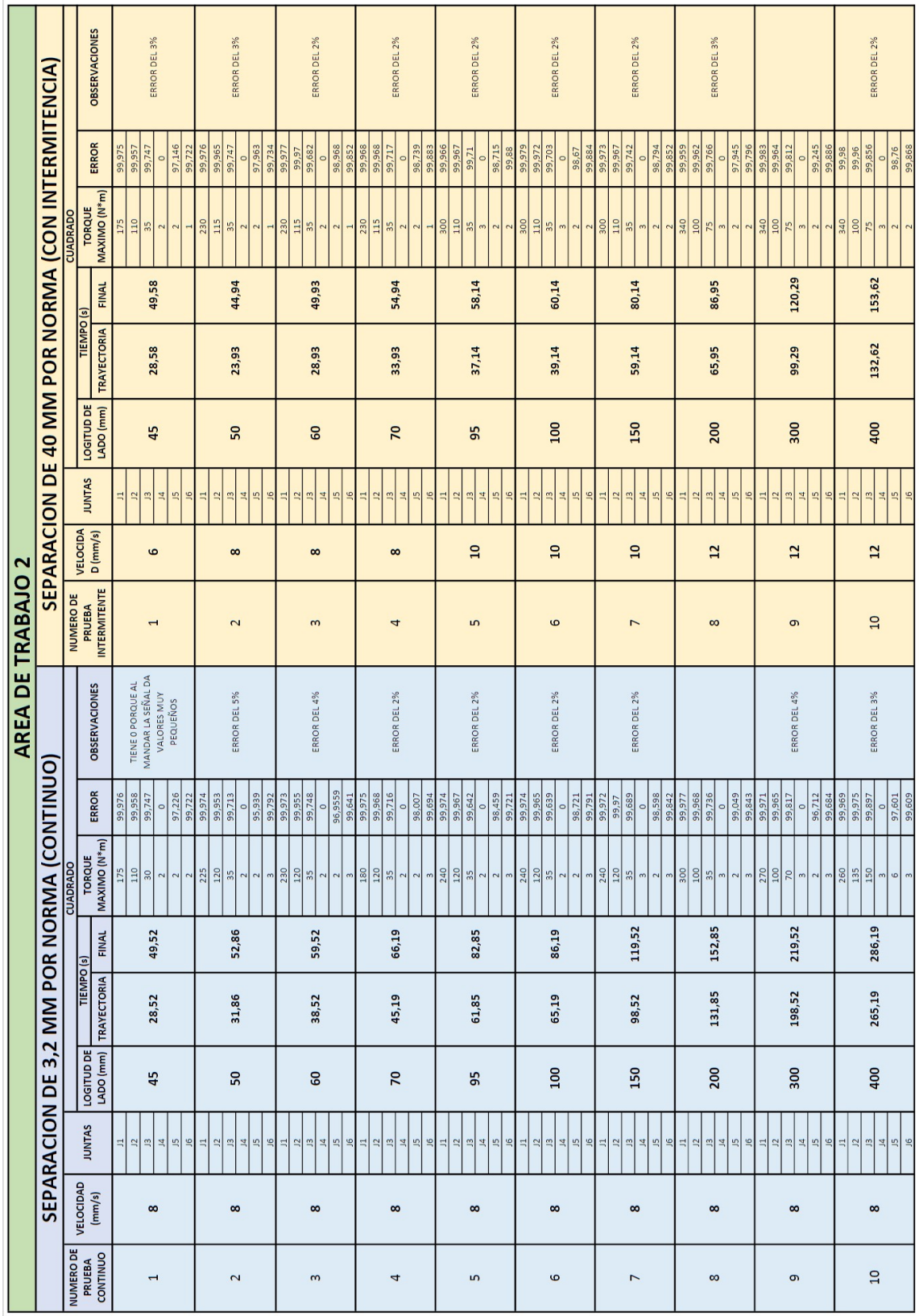

AREA DE TRABAJO 2																							
SEPARACION DE 3,2 MM POR NORMA (CONTINUO)									SEPARACION DE 40 MM POR NORMA (CON INTERMITENCIA)														
NUMERO DE PRUEBA CONTINUO	VELOCIDAD (mm/s)	JUNTAS	LOGITUD DE LADO (mm)	TIEMPO (s)		CUADRADO		OBSERVACIONES	NUMERO DE PRUEBA INTERMITENTE	VELOCIDAD (mm/s)	JUNTAS	LOGITUD DE LADO (mm)	TIEMPO (s)		CUADRADO		OBSERVACIONES
				TRAYECTORIA	FINAL	TORQUE MAXIMO (N*m)	ERROR						TRAYECTORIA	FINAL	TORQUE MAXIMO (N*m)	ERROR	
1	8	J1	45	28,52	49,52	175	99,976	TIENE 0 PORQUE AL MANDAR LA SEÑAL DA VALORES MUY PEQUEÑOS	1	6	J1	45	28,58	49,58	175	99,975	ERROR DEL 3%
		J2				110	99,958				J2				110	99,957	
		J3				30	99,747				J3				35	99,747	
		J4				2	0				J4				2	0	
		J5				2	97,226				J5				2	97,146	
		J6				2	99,722				J6				1	99,722	
2	8	J1	50	31,86	52,86	225	99,974	ERROR DEL 5%	2	8	J1	50	23,93	44,94	230	99,976	ERROR DEL 3%
		J2				120	99,953				J2				115	99,965	
		J3				35	99,713				J3				35	99,747	
		J4				2	0				J4				2	97,963	
		J5				2	95,939				J5				2	0	
		J6				3	99,792				J6				1	99,734	
3	8	J1	60	38,52	59,52	230	99,973	ERROR DEL 4%	3	8	J1	60	28,93	49,93	230	99,977	ERROR DEL 2%
		J2				120	99,955				J2				115	99,97	
		J3				35	99,748				J3				35	99,682	
		J4				2	0				J4				2	0	
		J5				2	96,9559				J5				2	98,968	
		J6				3	99,641				J6				1	99,852	
4	8	J1	70	45,19	66,19	180	99,975	ERROR DEL 2%	4	8	J1	70	33,93	54,94	230	99,968	ERROR DEL 2%
		J2				120	99,968				J2				115	99,968	
		J3				35	99,716				J3				35	99,717	
		J4				2	0				J4				2	0	
		J5				2	98,007				J5				2	98,739	
		J6				3	99,694				J6				1	99,883	
5	8	J1	95	61,85	82,85	240	99,974	ERROR DEL 2%	5	10	J1	95	37,14	58,14	300	99,966	ERROR DEL 2%
		J2				120	99,967				J2				110	99,967	
		J3				35	99,642				J3				35	99,71	
		J4				2	0				J4				3	0	
		J5				2	98,459				J5				2	98,715	
		J6				3	99,721				J6				2	99,88	
6	8	J1	100	65,19	86,19	240	99,974	ERROR DEL 2%	6	10	J1	100	39,14	60,14	300	99,979	ERROR DEL 2%
		J2				120	99,965				J2				110	99,972	
		J3				35	99,639				J3				35	99,703	
		J4				2	0				J4				3	0	
		J5				2	98,721				J5				2	98,67	
		J6				3	99,791				J6				2	99,884	
7	8	J1	150	98,52	119,52	240	99,972	ERROR DEL 2%	7	10	J1	150	59,14	80,14	300	99,973	ERROR DEL 2%
		J2				120	99,97				J2				110	99,967	
		J3				35	99,689				J3				35	99,742	
		J4				3	0				J4				3	0	
		J5				2	98,598				J5				2	98,794	
		J6				3	99,842				J6				2	99,852	
8	8	J1	200	131,85	152,85	300	99,977		8	12	J1	200	65,95	86,95	340	99,959	ERROR DEL 3%
		J2				100	99,968				J2				100	99,962	
		J3				35	99,736				J3				75	99,766	
		J4				3	0				J4				3	0	
		J5				2	99,049				J5				2	97,945	
		J6				3	99,843				J6				2	99,796	
9	8	J1	300	198,52	219,52	270	99,971	ERROR DEL 4%	9	12	J1	300	99,29	120,29	340	99,983	
		J2				100	99,965				J2				100	99,964	
		J3				70	99,817				J3				75	99,812	
		J4				3	0				J4				3	0	
		J5				2	96,712				J5				2	99,245	
		J6				3	99,684				J6				2	99,886	
10	8	J1	400	265,19	286,19	260	99,969	ERROR DEL 3%	10	12	J1	400	132,62	153,62	340	99,98	ERROR DEL 2%
		J2				135	99,975				J2				100	99,96	
		J3				150	99,897				J3				75	99,856	
		J4				3	0				J4				3	0	
		J5				6	97,601				J5				2	98,76	
		J6				3	99,609				J6				2	99,868	

TABLE B.3

Simulation results for the Linear trajectory (Workspace 2).

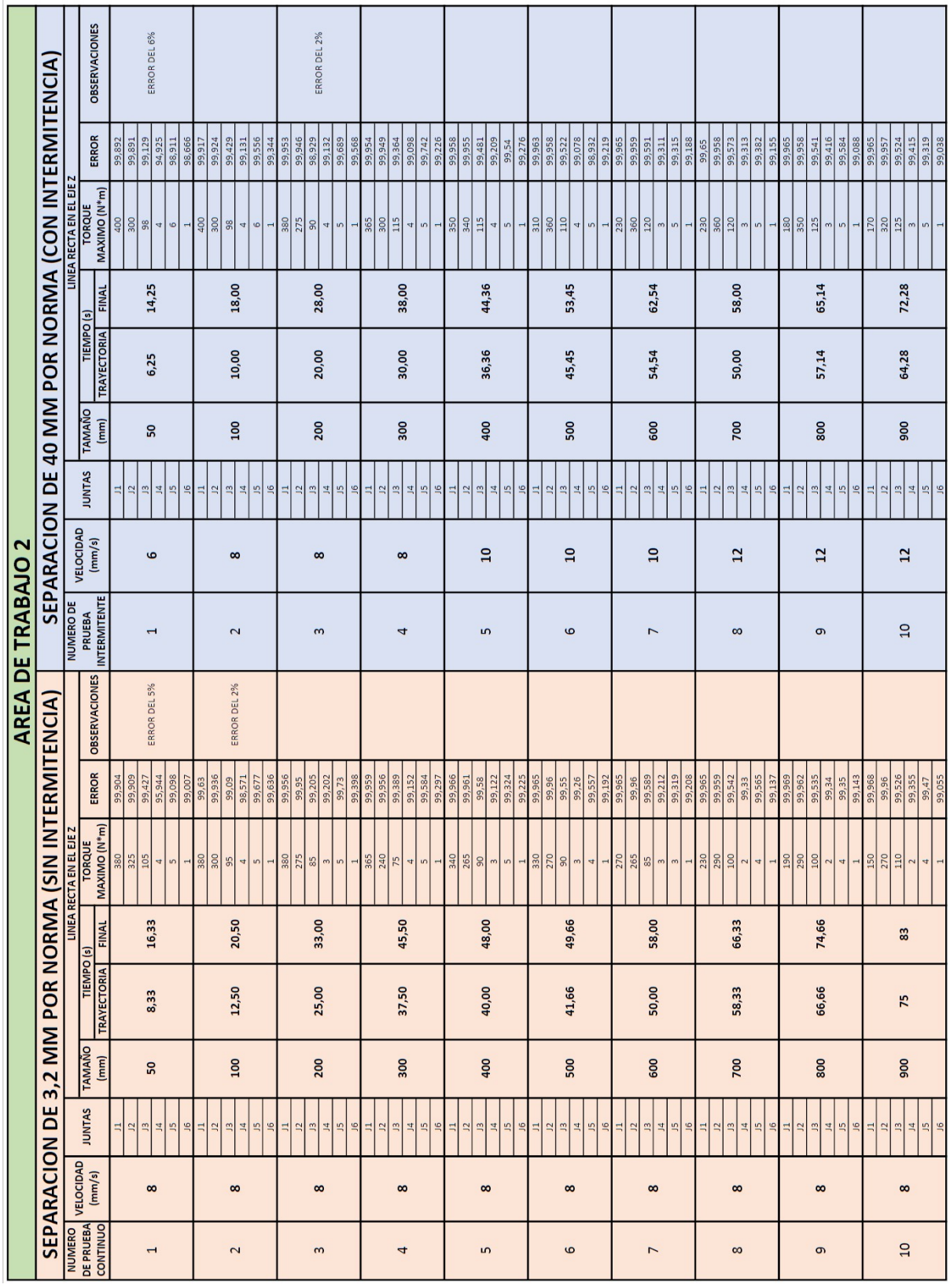

AREA DE TRABAJO 2																							
SEPARACION DE 3,2 MM POR NORMA (SIN INTERMITENCIA)									SEPARACION DE 40 MM POR NORMA (CON INTERMITENCIA)														
NUMERO DE PRUEBA CONTINUO	VELOCIDAD (mm/s)	JUNTAS	TAMAÑO (mm)	LINEA RECTA EN EL EJE Z				OBSERVACIONES	NUMERO DE PRUEBA INTERMITENTE	VELOCIDAD (mm/s)	JUNTAS	TAMAÑO (mm)	LINEA RECTA EN EL EJE Z										
				TIEMPO (s)		TORQUE MAXIMO (N*m)	ERROR						TIEMPO (s)		TORQUE MAXIMO (N*m)	ERROR	OBSERVACIONES						
				TRAYECTORIA	FINAL								TRAYECTORIA	FINAL									
1	8	J1	50	8,33	16,33	380	99,904	ERROR DEL 5%	1	6	J1	50	6,25	14,25	400	99,892	ERROR DEL 6%						
		J2				325	99,909				J2				300	99,891							
		J3				105	99,427				J3				98	99,129							
		J4				4	95,944				J4				4	94,925							
		J5				5	99,098				J5				6	96,911							
		J6				1	99,007				J6				1	98,666							
2	8	J1	100	12,50	20,50	380	99,63	ERROR DEL 2%	2	8	J1	100	10,00	18,00	400	99,917							
		J2				300	99,936				J2				300	99,924							
		J3				95	99,09				J3				98	99,429							
		J4				4	98,571				J4				4	99,131							
		J5				5	99,677				J5				6	95,556							
		J6				1	99,636				J6				1	99,344							
3	8	J1	200	25,00	33,00	380	99,956		3	8	J1	200	20,00	28,00	380	99,953	ERROR DEL 2%						
		J2				275	99,95				J2				275	99,946							
		J3				85	99,205				J3				90	98,929							
		J4				3	99,202				J4				4	99,132							
		J5				5	99,73				J5				5	99,689							
		J6				1	99,398				J6				1	99,568							
4	8	J1	300	37,50	45,50	365	99,959		4	8	J1	300	30,00	38,00	365	99,954							
		J2				240	99,956				J2				300	99,949							
		J3				75	99,389				J3				115	99,364							
		J4				4	99,152				J4				4	99,098							
		J5				5	99,584				J5				5	99,742							
		J6				1	99,297				J6				1	99,226							
5	8	J1	400	40,00	48,00	340	99,966		5	10	J1	400	36,36	44,36	350	99,958							
		J2				265	99,961				J2				340	99,955							
		J3				90	99,58				J3				115	99,481							
		J4				3	99,122				J4				4	99,209							
		J5				5	99,324				J5				5	99,54							
		J6				1	99,225				J6				1	99,276							
6	8	J1	500	41,66	49,66	330	99,965		6	10	J1	500	45,45	53,45	310	99,963							
		J2				270	99,96				J2				360	99,958							
		J3				90	99,55				J3				110	99,522							
		J4				3	99,26				J4				4	99,078							
		J5				4	99,557				J5				5	96,932							
		J6				1	99,192				J6				1	99,219							
7	8	J1	600	50,00	58,00	270	99,965		7	10	J1	600	54,54	62,54	230	99,965							
		J2				265	99,96				J2				360	99,959							
		J3				85	99,589				J3				120	99,591							
		J4				3	99,212				J4				3	99,311							
		J5				3	99,319				J5				5	99,315							
		J6				1	99,208				J6				1	99,188							
8	8	J1	700	58,33	66,33	230	99,965		8	12	J1	700	50,00	58,00	230	99,65							
		J2				290	99,959				J2				360	99,958							
		J3				100	99,542				J3				120	99,573							
		J4				2	99,33				J4				3	99,313							
		J5				4	99,565				J5				5	99,382							
		J6				1	99,137				J6				1	99,155							
9	8	J1	800	66,66	74,66	190	99,969		9	12	J1	800	57,14	65,14	180	99,965							
		J2				290	99,962				J2				350	99,958							
		J3				100	99,535				J3				125	99,541							
		J4				2	99,34				J4				3	99,416							
		J5				4	99,35				J5				5	99,584							
		J6				1	99,143				J6				1	99,088							
10	8	J1	900	75	83	150	99,968		10	12	J1	900	64,28	72,28	170	99,965							
		J2				270	99,96				J2				320	99,957							
		J3				110	99,526				J3				125	99,524							
		J4				2	99,355				J4				3	99,415							
		J5				4	99,47				J5				5	99,319							
		J6				1	99,055				J6				1	99,038							

APPENDIX B

D.U.M.-E ROBOTIC ARM PLANS

D.U.M.E. (Digital Unit for MIG Experimentation)

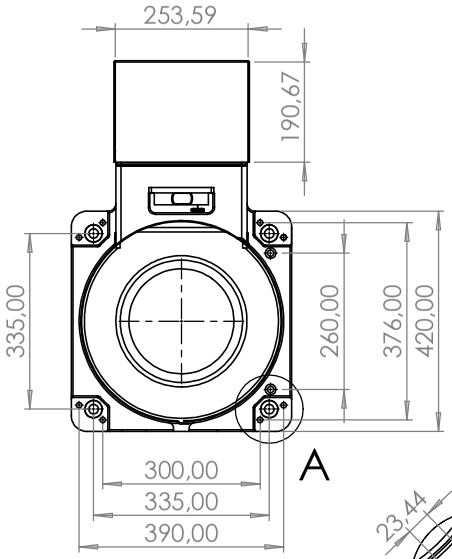

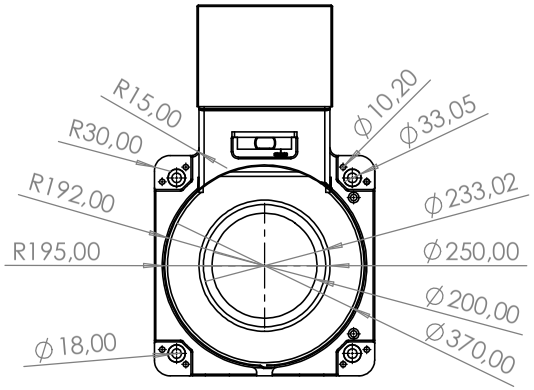

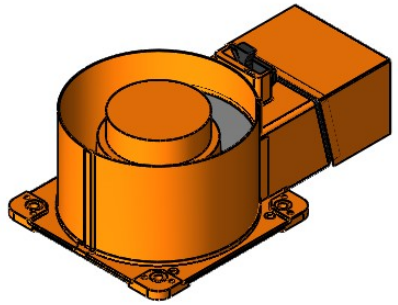

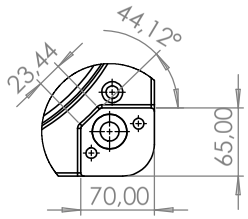

DETALLE A

ESCALA 1 : 5

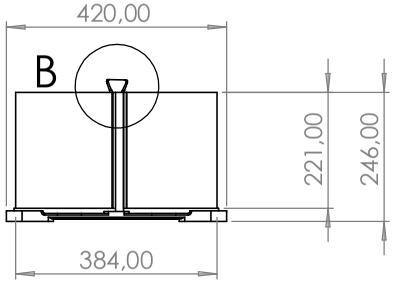

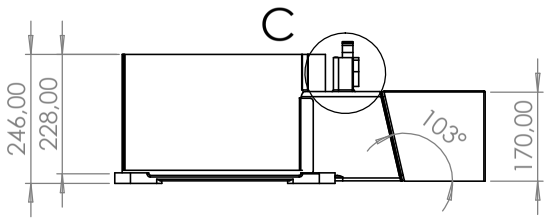

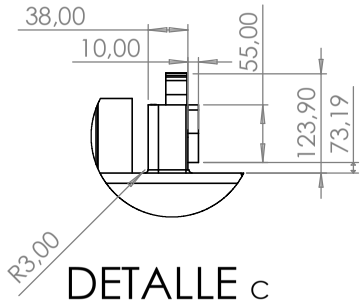

DETALLE C

ESCALA 1 : 5

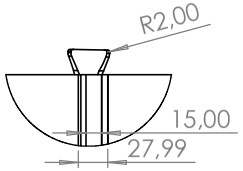

DETALLE B

ESCALA 1 : 5

NOTAS GENERALES/GENERAL NOTES:	REGISTRO/REGISTER:	FECHA/DATE:
	DIBUJANTE/DRAFTMAN: José Arévalo	06/01/2026
	DISEÑADOR/DESIGNER: José Arévalo	06/01/2026
	REVISADO/REVIEWED BY: Guillermo Mosquera	06/01/2026
	REVISADO/REVIEWED BY: Guillermo Mosquera	06/01/2026

UNIVERSIDAD INTERNACIONAL DEL ECUADOR

ESCUELA DE INGENIERIA MECATRONICA

ASIGNATURA/SUBJECT: Seminario de Integración Curricular

PROYECTO/PROYECT: D.U.M.-E: PROTOTYPE OF A ROBOTIC WELDING ARM

DESCRIPCION/DESCRIPTION: BASE PIECE

TAMAÑO/PAPER SIZE: A4

ESCALA/SCALE: 1:1

DIBUJO Nº/DRAWING Nº: DM-001

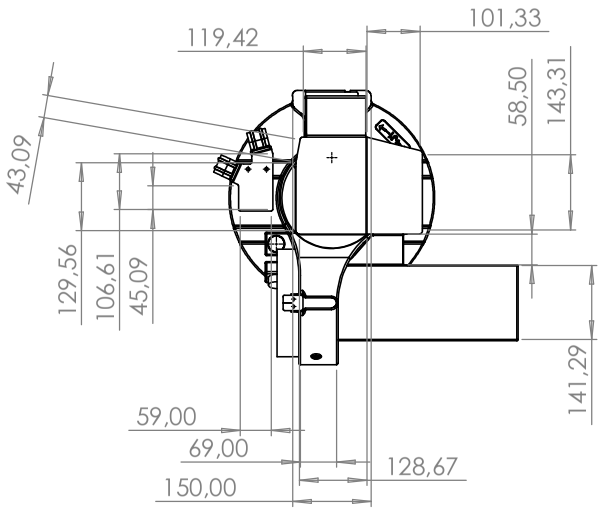

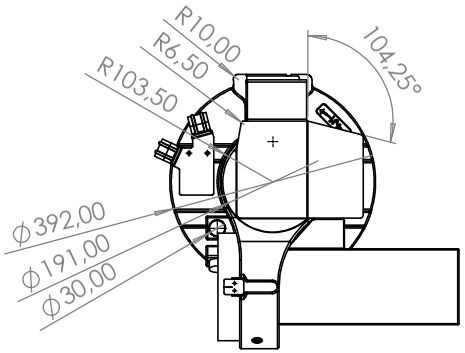

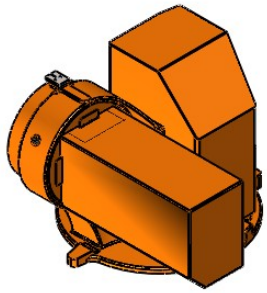

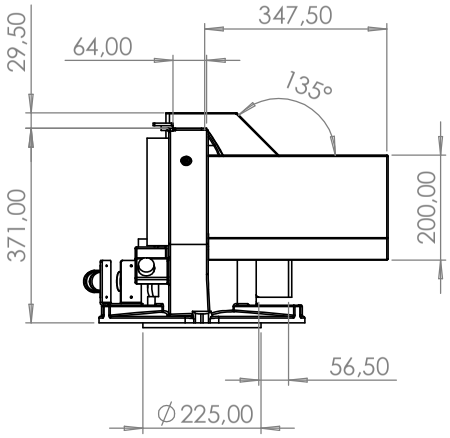

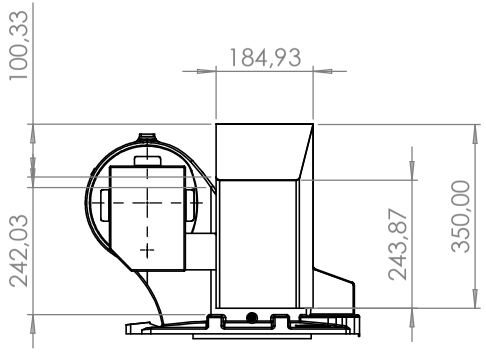

NOTAS GENERALES/GENERAL NOTES:	REGISTRO/REGISTER:	FECHA/DATE:	UNIVERSIDAD INTERNACIONAL DEL ECUADOR ESCUELA DE INGENIERIA MECATRONICA	
	DIBUJANTE/DRAFTMAN: José Arévalo	06/01/2026	ASIGNATURA/SUBJECT: Seminario de Integración Curricular	
	DISEÑADOR/DESIGNER: José Arévalo	06/01/2026	PROYECTO/PROYECT: D.U.M.-E: PROTOTYPE OF A ROBOTIC WELDING ARM	
	REVISADO/REVIEWED BY: Guillermo Mosquera	06/01/2026	DESCRIPCION/DESCRIPTION: WAIST PIECE	
	REVISADO/REVIEWED BY: Guillermo Mosquera	06/01/2026	TAMAÑO/PAPER SIZE: A4 ESCALA/SCALE: 1:1	DIBUJO N°/DRAWING N°: DM-002

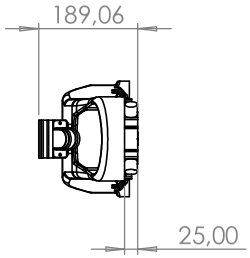

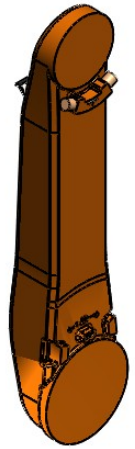

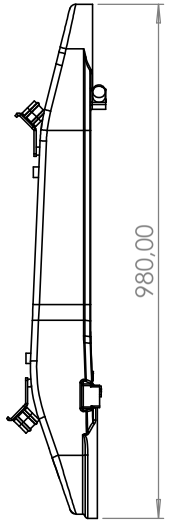

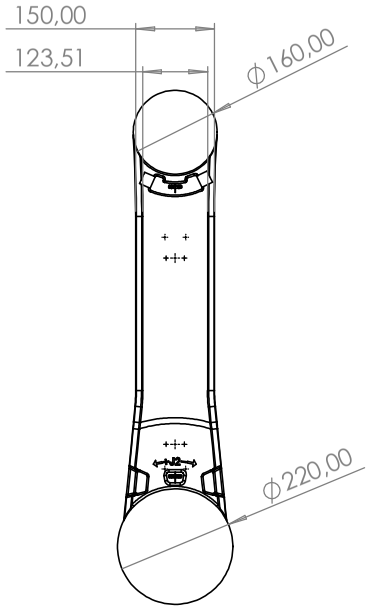

NOTAS GENERALES/GENERAL NOTES:	REGISTRO/REGISTER:	FECHA/DATE:	UNIVERSIDAD INTERNACIONAL DEL ECUADOR ESCUELA DE INGENIERIA MECATRONICA
	DIBUJANTE/DRAFTMAN: José Arévalo	06/01/2026	ASIGNATURA/SUBJECT: Seminario de Integración Curricular
	DISEÑADOR/DESIGNER: José Arévalo	06/01/2026	PROYECTO/PROYECT: D.U.M.-E: PROTOTYPE OF A ROBOTIC WELDING ARM
	REVISADO/REVIEWED BY: Guillermo Mosquera	06/01/2026	DESCRIPCION/DESCRIPTION: SHOULDER PIECE
	REVISADO/REVIEWED BY: Guillermo Mosquera	06/01/2026	TAMAÑO/PAPER SIZE: A4 ESCALA/SCALE: 1:1
			DIBUJO N°/DRAWING N°: DM-003

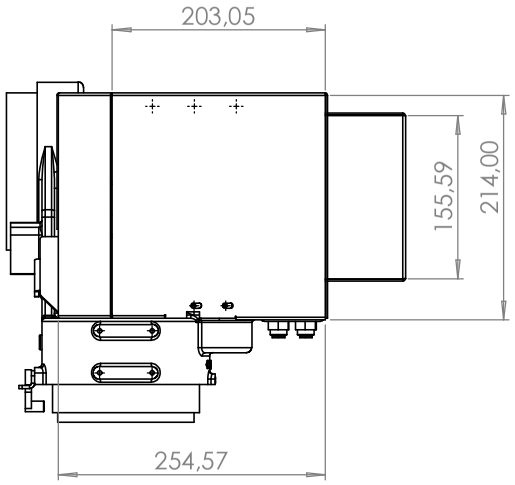

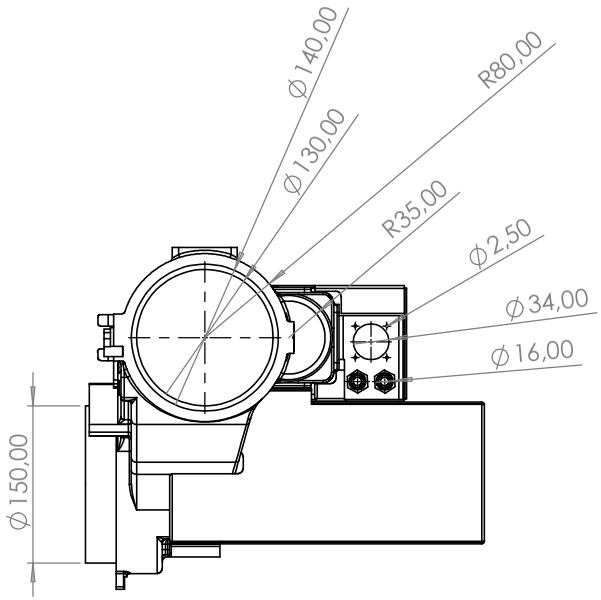

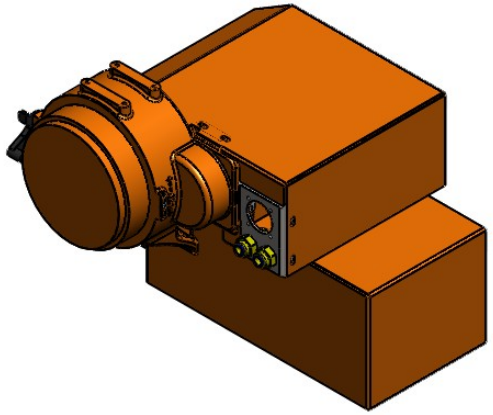

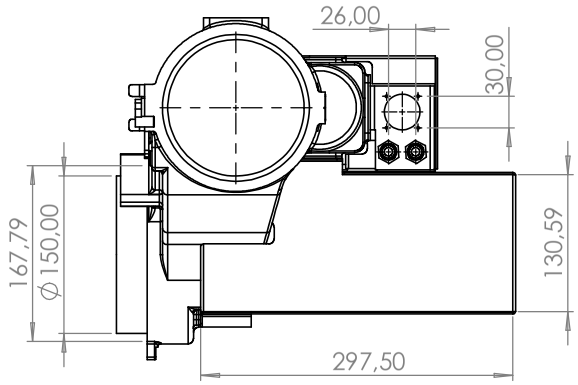

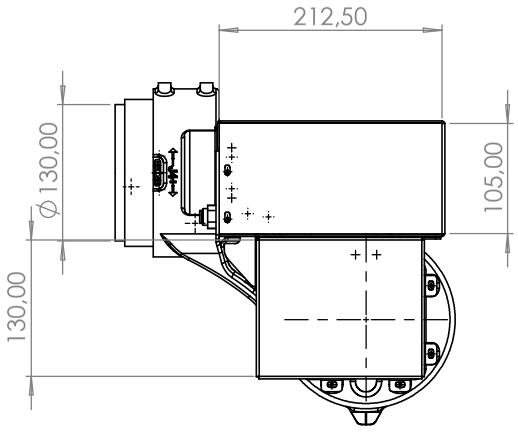

NOTAS GENERALES/GENERAL NOTES:	REGISTRO/REGISTER:	FECHA/DATE:
	DIBUJANTE/DRAFTMAN: José Arévalo	06/01/2026
	DISEÑADOR/DESIGNER: José Arévalo	06/01/2026
	REVISADO/REVIEWED BY: Guillermo Mosquera	06/01/2026
	REVISADO/REVIEWED BY: Guillermo Mosquera	06/01/2026

UNIVERSIDAD INTERNACIONAL DEL ECUADOR
ESCUELA DE INGENIERIA MECATRONICA

ASIGNATURA/SUBJECT: Seminario de Integración Curricular

PROYECTO/PROYECT: D.U.M.-E: PROTOTYPE OF A ROBOTIC WELDING ARM

DESCRIPCION/DESCRIPTION: ELBOW PIECE

TAMAÑO/PAPER SIZE: A4

ESCALA/SCALE: 1:1

DIBUJO N°/DRAWING N°: DM-004

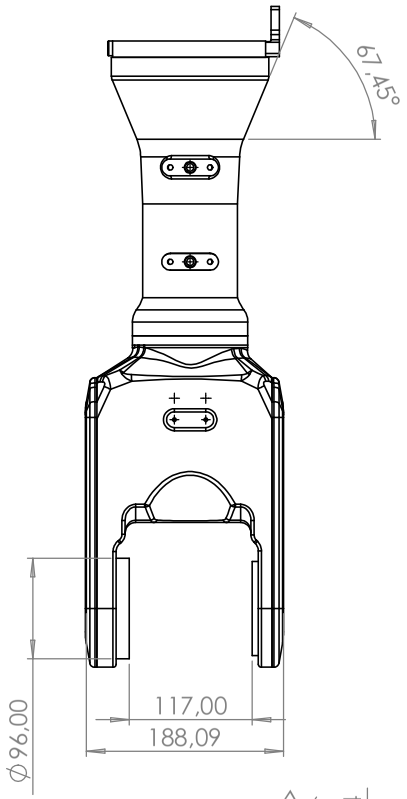

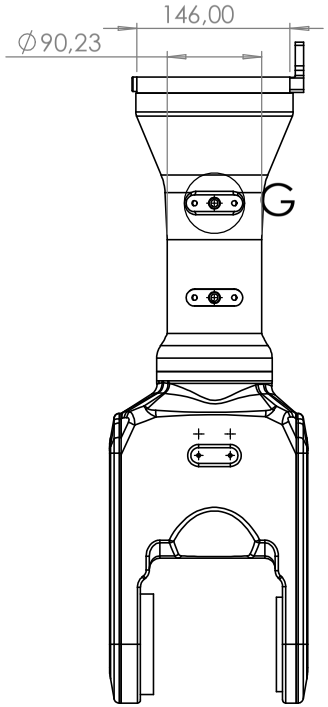

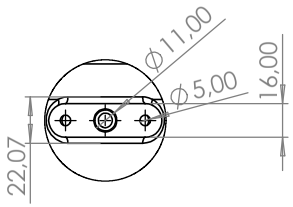

DETALLE G

ESCALA 2 : 5

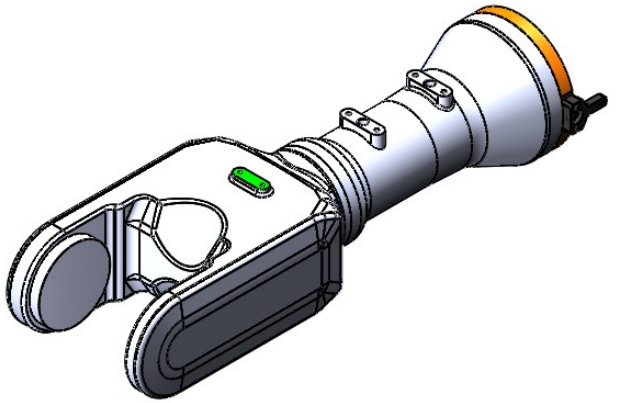

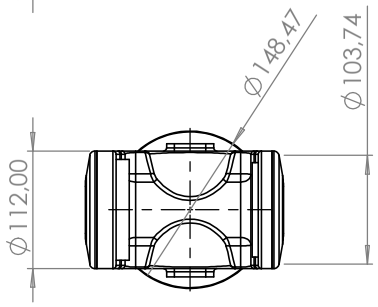

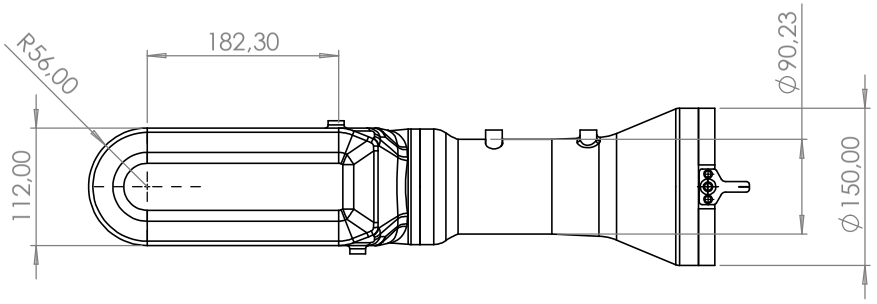

NOTAS GENERALES/GENERAL NOTES:	REGISTRO/REGISTER:	FECHA/DATE:
	DIBUJANTE/DRAFTMAN: José Arévalo	06/01/2026
	DISEÑADOR/DESIGNER: José Arévalo	06/01/2026
	REVISADO/REVIEWED BY: Guillermo Mosquera	06/01/2026
	REVISADO/REVIEWED BY: Guillermo Mosquera	06/01/2026

TAMAÑO/PAPER SIZE: A4

ESCALA/SCALE: 1:1

UNIVERSIDAD INTERNACIONAL DEL ECUADOR

ESCUELA DE INGENIERIA MECATRONICA

ASIGNATURA/SUBJECT: Seminario de Integración Curricular

PROYECTO/PROYECT: D.U.M.-E: PROTOTYPE OF A ROBOTIC WELDING ARM

DESCRIPCION/DESCRIPTION: FOREARM PIECE

DIBUJO N°/DRAWING N°: DM-005

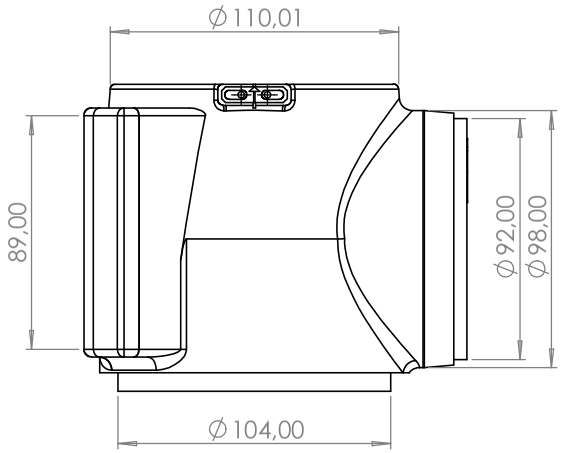

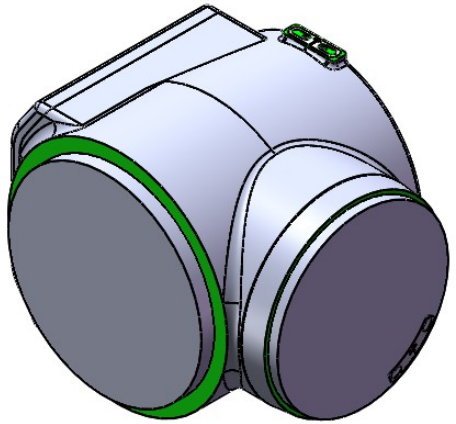

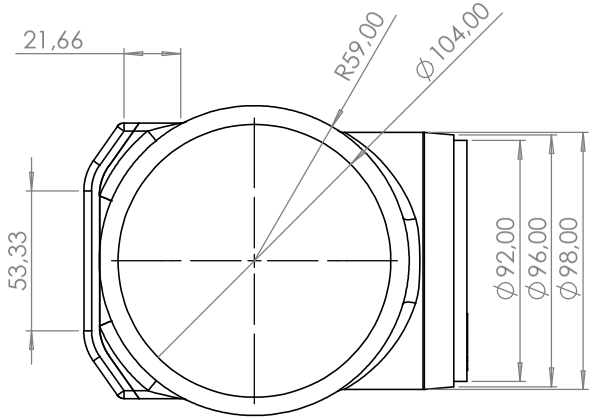

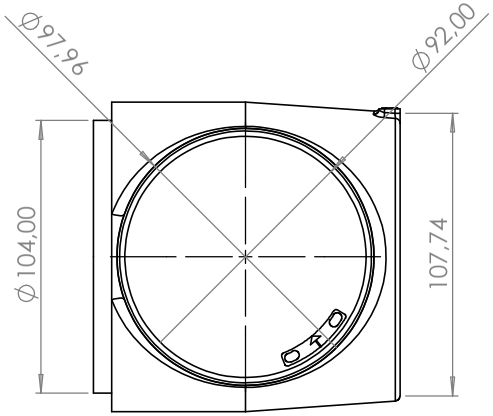

NOTAS GENERALES/GENERAL NOTES:	REGISTRO/REGISTER:	FECHA/DATE:	UNIVERSIDAD INTERNACIONAL DEL ECUADOR ESCUELA DE INGENIERIA MECATRONICA
	DIBUJANTE/DRAFTMAN: José Arévalo	06/01/2026	ASIGNATURA/SUBJECT: Seminario de Integración Curricular
	DISEÑADOR/DESIGNER: José Arévalo	06/01/2026	PROYECTO/PROYECT: D.U.M.-E: PROTOTYPE OF A ROBOTIC WELDING ARM
	REVISADO/REVIEWED BY: Guillermo Mosquera	06/01/2026	DESCRIPCION/DESCRIPTION: DOLL PIECE
	REVISADO/REVIEWED BY: Guillermo Mosquera	06/01/2026	TAMAÑO/PAPER SIZE: A4 ESCALA/SCALE: 1:1 DIBUJO N°/DRAWING N°: DM-006

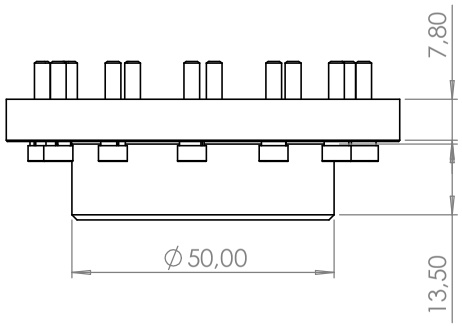

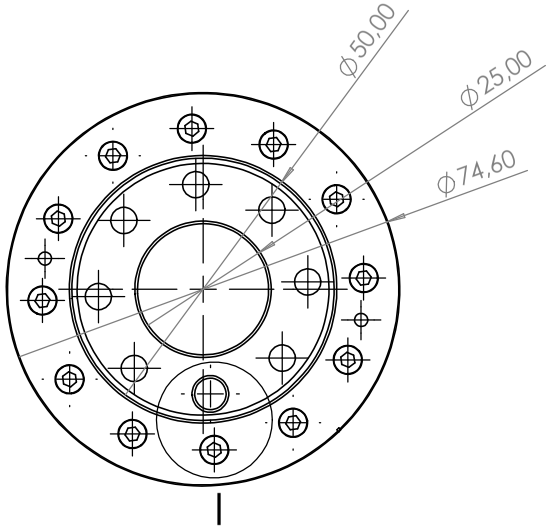

I

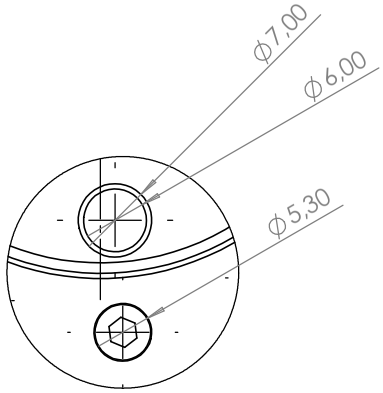

DETALLE I
ESCALA 2 : 1

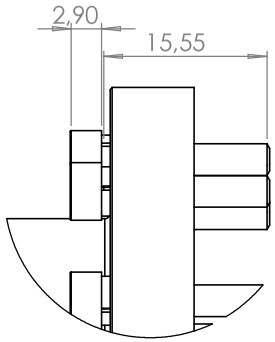

DETALLE J
ESCALA 2 : 1

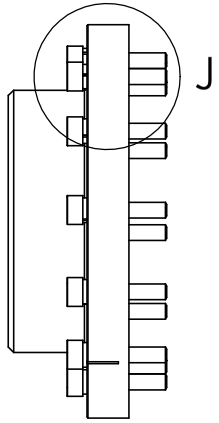

NOTAS GENERALES/GENERAL NOTES:	REGISTRO/REGISTER:	FECHA/DATE:	UNIVERSIDAD INTERNACIONAL DEL ECUADOR ESCUELA DE INGENIERIA MECATRONICA
	DIBUJANTE/DRAFTMAN: José Arévalo	06/01/2026	ASIGNATURA/SUBJECT: Seminario de Integración Curricular
	DISEÑADOR/DESIGNER: José Arévalo	06/01/2026	PROYECTO/PROYECT: D.U.M.-E: PROTOTYPE OF A ROBOTIC WELDING ARM
	REVISADO/REVIEWED BY: Guillermo Mosquera	06/01/2026	DESCRIPCION/DESCRIPTION: HAND PIECE
	REVISADO/REVIEWED BY: Guillermo Mosquera	06/01/2026	TAMAÑO/PAPER SIZE: A4 ESCALA/SCALE: 1:1 DIBUJO N°/DRAWING N°: DM-007